目　　录

目　　录 ····· V

1 Introduction ····· **1**

1.1 Background information ····· 1

1.2 Purpose of this thesis ····· 3

2 Two-leg ladder Hubbard model ····· **5**

2.1 Hamiltonian ····· 5

2.2 SO(8) symmetry of the two-leg ladder model ····· 7

3 Renormalization group and its extension ····· **11**

3.1 Basic ideas of renormalization group ····· 11

3.2 Wilsonian renormalization group ····· 13

3.2.1 General procedure ····· 13

3.2.2 Applying to two-leg ladder model ····· 16

3.3 Functional renormalization group ····· 19

3.3.1 Useful functionals ····· 19

3.3.2 Regulator ····· 21

3.3.3 SU(2) invariant system ····· 22

3.4 Singular-mode functional renormalization group ····· 23

3.4.1 Projection of channels ····· 26

4 Numerical calculation and results ····· **29**

4.1 N-patch functional renormalization group ····· 29

4.2 Singular-mode renormalization group method ····· 31

4.3 Results and analysis of the data from FRG ····· 33

4.3.1 Arrange the vertex functions into channels ····· 33

4.3.2 Arrange the vertex functions into current representation ····· 37
4.4 Results from SMFRG ····· 39
4.4.1 SMFRG on two-leg ladder system ····· 40
4.4.2 SMFRG on 1d chain ····· 41
4.4.3 Calculation errors ····· 43

5 Conclusion ····· 45
5.1 Summary of implementation of FRG and SMFRG ····· 45
5.2 Summary of two-leg ladder Hubbard model ····· 46

参考文献 ····· **47**

致　　谢 ····· **51**

Introduction

Background information

The discovery of high-T_c superconductors challenges the conventional BCS theory. The lack of phonon-mediated interaction and quasi-particle description in their normal state makes the system hard to investigate and understand. These challenges lead to the investigation of other pairing mechanism and non-Fermi liquid behavior[1,2]. Cuprate superconductors are predominant and were firstly discovered in 1986[3], the T_c record of this type of superconductors reaches 130 K[4]. Hence, the understanding of the high-T_c superconductivity may assist to find the room temperature superconductor.

The cuprate superconductors, such as YBCO and BSCCO, have layered structure, the Cu-O_2 planes are sandwiched by other elements which are less interesting. The Cu-O_2 planes are responsible for the superconductivity. The electronic state of the superconducting Cu-O_2 planes arises from the Cu $d_{x^2-y^2}$ orbital and two oxygen p orbital[5]. To describe the electronic state, three-band model is too complicated, but the low energy state can actually be described by one-band model due to the essential insight known as the Zhang-Rice singlet (the spin of the doped hole combines with the spin on the Cu to form a spin singlet)[6]. Therefore, the nature of the conventional superconductivity now arises from a relatively simple 2d one-band Hubbard model.

The strong interaction limit of the Hubbard model on a square lattice leads to the $t-J$ model and is used to describe the electrons on such planes. The strong on-site interaction in the $t-J$ model leads to the Mott insulator at lower doping level. This type of the Mott insulator with the presence of the magnetic order is antiferromagnetic because the virtual hopping favors the antiferromagnetic spin configuration. When increasing the doping level, the antiferromagnetic order is broken and the materials become superconductors[5]. One can view the unconventional superconductivity arises from doping the Mott insulator.

Below the optimal doping, some experiments showed that there are signs of spin gap opening at temperature above the transition to the superconducting phase[7,8]. The spin gap implied a strong connection to the superconductivity. It motivates to find the spin-liquid Mott insulator, where no broken symmetry exists, the magnetic order is short ranged and the spin gap occurs[9].

As previously introduced, the lattice of most cuprate superconductors is 2d square lattice. The lattice seems to be simple but hard to solve the Hubbard model on such lattice even numerically. Quantum Monte Carlo methods have "sign problem" for the fermion system[10], thus the results are inconvincible; density matrix renormalization group method cannot be applied to 2d lattice, but can solve the model on a quasi-1d lattice[11]; random phase approximation and renormalization group can be used for tiny interaction but not for the moderate value. Functional renormalization group treats each interaction on equal footing at each energy scale and this method on 2d square lattice Hubbard model produced reasonable results but the computational costs are huge[12,13].

The difficulty in solving higher dimension Hubbard model and its underlying connection to the unconventional superconductivity motivate us to investigate the two-leg ladder Hubbard model. It turns out to be a relatively simple model to produce the unconventional superconductivity, and promising to find the spin liquid Mott insulator. Previous works suggested that it is an integrable model with numerous analytical results[9,14]. At half-filling, the Mott insulating phase is described by a Heisenberg antiferromagnet, and due to the tendency to forming singlet bond across the rungs of the ladder, the spin-liquid behavior is expected[8,15].

The two-leg ladder Hubbard model has surprising low energy behavior. Upon the renormalization flow, the ratio of different coupling constants is a fixed value and the low energy effective Hamiltonian of the two-leg ladder Hubbard model can be described by a SO(8) Gross-Neveu (GN) model[9]. The excitations of SO(8) GN model can be arranged into SO(8) multiplets. Each of the excitations is separated from the ground state by a non-zero gap. One vector multiplet consists of collective two-particle excitations: two charge ±2e "Cooper pairs" around zero momentum, a triplet of spin-one "magnons" around momentum $(-\pi, \pi)$, and three neutral spin-zero "charge-density-

wave" (or particle-hole pair) excitations. SO(8) transformations rotate the components of the vector into one another, unifying the pair, magnon, and charge-density-wave excitations[16].

We would like to use functional renormalization group method in our analysis on two-leg ladder Hubbard model. In general, superconductivity is a low energy phenomenon ($\sim meV$), compared with the Coulomb repulsion ($\sim eV$) and magnetic interaction ($\sim 0.1eV$). The renormalization group method is the powerful method to find the low energy effective theory of the system. For fermion system, the coupling constant is coupling functions dependent on the momentum and frequency[17]. The introduced regulator enables the flow equation smooth and step-by-step removes the high energy part, and leads the model to its low energy effective version where the low energy orders, such as superconductivity, spin-density-wave, and charge-density-wave emerge[18].

Purpose of this thesis

In this thesis, the purposes are twofold. For one purpose, we would like to thoroughly investigate the low energy behavior of the two-leg ladder Hubbard model and compare with the previous work, for example, whether this model develops superconductivity, whether the proposed SO(8) symmetry of the interactions and spin gap exists[9]. For another purpose, we would like to understand, apply and develop the numerical method to investigate such strongly interacting system.

The Hubbard model in two-leg ladder lattice is a quasi-1d model. Because of the Hubbard term, it is hard to use simple mean field or other methods to investigate. The Hubbard term in this model can be dissected into forward, backward and umklapp scattering. There exist 9 independent couplings, 4 for backward scattering, 2 for forward scattering and 3 for umklapp scattering. The flow to low energy effective action leads 7 of the 9 independent couplings to diverge in the constant ratio and 2 remain small. This feature makes the low energy effective theory of the model can be mapped to typical SO(8) Gross-Neveu model which has the SO(8) symmetry. The two-leg ladder Hubbard model can also be exactly mapped to its bosonization dual and the symmetry

manifests (but not SO(8))[9].

However, the naive renormalization group method in the previous work doesn't contain and consider enough information of the momentum space. Functional renormalization group in a finer grid of the momentum space shows the deviation from the exact SO(8) symmetry. Take more and more patches into consideration, the interactions blow up before divergence and deviate from the "ray" like feature. Besides the functional renormalization group, we also apply the advanced singular-mode functional renormalization group to this system[19,20]. In the following sections, the detailed implementations will be discussed.

The thesis is structured as we first write down the Hamiltonian and explain the SO(8) symmetry of such model in chapter. 2. The renormalization group, functional renormalization group, and singular mode renormalization group method are detailed introduced in chapter. 3. In chapter. 4, we present our numerical results from different schemes and compared with the analytical results.

Two-leg ladder Hubbard model

Hamiltonian

The Hamiltonian of the free electron model on the two-leg ladder lattice is,

$$H_0 = \sum_{x,\alpha} \left(-t a_{1\alpha}^{\dagger}(x+1)\, a_{1\alpha}(x) + (1 \to 2) - t_{\perp} a_{1\alpha}^{\dagger}(x)\, a_{2\alpha}(x) + H.c. \right), \tag{2-1}$$

where $a_{i\alpha}^{\dagger}, a_{i\alpha}$ are the creation and annihilation operators on band i with spin indice α, t is the hopping constant of the intra-band and $t_{\perp}$ is the hopping constant of the inter-band, x is the position and $H.c.$ represents hermitian conjugate. The Hamiltonian can be transformed into band representation by introducing $c_{i,\alpha} = \left[a_{1,\alpha} + (-1)^i a_{2,\alpha} \right] / \sqrt{2}$. Thus, in the band representation, the Hamiltonian is,

$$\begin{aligned} H_0 = & \sum_{x,\alpha} \left(-t \left(c_{1,\alpha}^{\dagger}(x+1)\, c_{1,\alpha}(x) + c_{2,\alpha}^{\dagger}(x+1)\, c_{2,\alpha}(x) \right) \right. \\ & \left. -t_{\perp} \left(-c_{1,\alpha}^{\dagger}(x)\, c_{1,\alpha}(x) + c_{2,\alpha}^{\dagger}(x)\, c_{2,\alpha}(x) \right) \right), \end{aligned} \tag{2-2}$$

Considering the Fourier transformation of the operators,

$$c_{i\sigma}^{\dagger}(x) = \frac{1}{\sqrt{N}} \sum_{k} e^{-ik\cdot x} c_{\sigma}^{\dagger}(k). \tag{2-3}$$

The Hamiltonian in momentum space is,

$$\begin{aligned} H_0 &= \sum_{k,\alpha} \left(-2t\cos k + t_{\perp} \right) c_{1,\alpha}^{\dagger} c_{1,\alpha} + \left(-2t\cos k - t_{\perp} \right) c_{2,\alpha}^{\dagger} c_{2,\alpha} \\ &= \sum_{k,\alpha} \xi_1(k)\, c_{1,\alpha}^{\dagger} c_{1,\alpha} + \xi_2(k)\, c_{2,\alpha}^{\dagger} c_{2,\alpha}, \end{aligned} \tag{2-4}$$

where $\xi_1(k) = -2t\cos k + t_{\perp}, \xi_2(k) = -2t\cos k - t_{\perp}$.

We focus on the half-filling case with one electron per site. We want the two bands to cross the Fermi surface, hence, we have $t_{\perp} < 2t$. The band structure can be linearized near the Fermi points and the Fermi velocities are the same for the two bands, namely

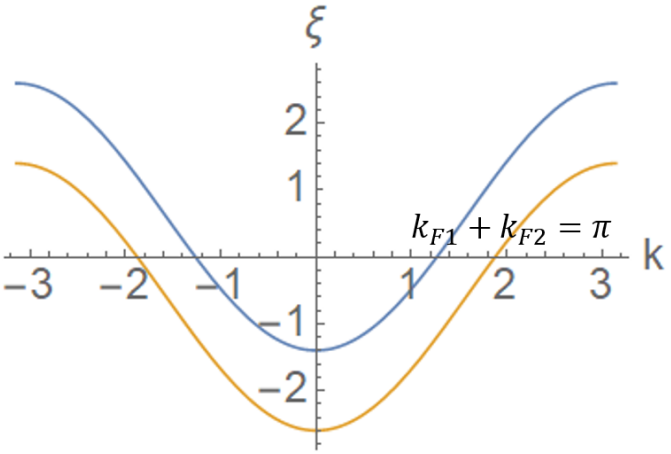

图 2-1: The band structure of the free fermion model.

$v = 2t \sin \arccos \frac{t_\perp}{2t}$,

$$H_0 = \sum_{\alpha,i=L,R} \int_{-\Lambda}^{\Lambda} \frac{dk_{1,2}}{2\pi} \left\{ v k_1 c^\dagger_{1i,\alpha} c_{1i,\alpha} + v k_2 c^\dagger_{2i,\alpha} c_{2i,\alpha} \right\}, \tag{2-5}$$

where $k_1 = |K| - K_{F1}, k_2 = |K| - K_{F2}$, K_{F1} and K_{F2} are the Fermi momenta of the anti-bonding and bonding bands. Till now, we have the free part of the total Hamiltonian which contains two bands with the same Fermi velocity. The total Hamiltonian also contains the strong interacting part, the Hubbard term,

$$H_{\text{int}} = U \sum_i : n_{i\uparrow} n_{j\downarrow} :, \tag{2-6}$$

where $n_{i\sigma} = c^\dagger_{i\sigma} c_{i\sigma}$ and $: \ldots :$ represents the normal order. The Hubbard term is essential for the system to develop superconducting order and other order, however, it is hard to solve. In the following sections, we will apply several different methods to this model and extract its low energy behavior.

SO(8) symmetry of the two-leg ladder model

To see the SO(8) symmetry, we would like to consider a typical form of the Hamiltonian. We first separate the left-moving and right-moving fermions by,

$$c_{i\alpha} \sim c_{Ri\alpha} e^{ik_{Fi}x} + c_{Li\alpha} e^{-ik_{Fi}x}.$$

In real space, the Eq. 2–5 becomes,

$$\mathcal{H}_0 = v \sum_{i,\alpha} c^\dagger_{Ri\alpha} i\partial_x c_{Ri\alpha} - c^\dagger_{Li\alpha} i\partial_x c_{Li\alpha}.$$

The indices $i\alpha$ can be grouped into a by, $(1\uparrow, 1\downarrow, 2\uparrow, 2\downarrow) \to (1,2,3,4)$, and we use $\psi_a = (c_{Ra}, c_{La})$,

$$H_0 = v \sum_a i\psi^\dagger_a \tau_z \partial_x \psi_a,$$

where τ_z is the z component of the Pauli matrices and the repeated indices mean summation.

The interaction term Eq. 2–6 can be expressed in terms of the currents, defined by,

$$J_{ij} = c^\dagger_{i\alpha} c_{j\alpha}, J^k_{ij} = \frac{1}{2} c^\dagger_{i\alpha} \sigma^k{}_{\alpha\beta} c_{j\beta}, \tag{2–7}$$

$$I_{ij} = c_{i\alpha} \epsilon_{\alpha\beta} c_{j\beta}, I^k_{ij} = \frac{1}{2} c_{i\alpha} (\epsilon\sigma^k)_{\alpha\beta} c_{j\beta}, \tag{2–8}$$

where the repeated Greek letters represents the summation over the spins, σ is the pauli matrix and ϵ is the two-rank Levi-Civita symbol. Therefore the two-particle interaction can be expressed as,

$$\begin{aligned} \mathcal{H}_I = {} & b^\rho_{ij} J_{Rij} J_{Lij} - b^\sigma_{ij} \mathbf{J}_{Rij} \cdot \mathbf{J}_{Lij} + f^\rho_{ij} J_{Rii} J_{Ljj} - f^\sigma_{ij} \mathbf{J}_{Rii} \cdot \mathbf{J}_{Ljj} \\ & + u^\rho_{ij} I^\dagger_{Rij} I_{L\hat{i}\hat{j}} - u^\sigma_{ij} \mathbf{I}^\dagger_{Rij} \cdot \mathbf{I}_{L\hat{i}\hat{j}} + H.c., \end{aligned} \tag{2–9}$$

where f, b and u denote the forward, backward and Umklapp scattering respectively, $\hat{1} = 2, \hat{2} = 1$. Because of the Hermiticity, $b_{12} = b_{21}$, and parity symmetry, $R \leftrightarrow L$, gives $f_{12} = f_{21}$. We also set $f_{ii} = 0$. At half-filling with particle-hole symmetry

$b_{11} = b_{22}$. Meanwhile, $u_{12} = u_{21}$ and we choose $u_{ii}^{\sigma} = 0$. Hence, the nine independent interactions are, $b_{11}^{\rho,\sigma}, b_{12}^{\rho,\sigma}, f_{12}^{\rho,\sigma}, u_{11}^{\sigma}, u_{12}^{\rho}, u_{12}^{\sigma}$.

Upon bosonization, the interaction term contains the competing cosine terms, which are hard to pin the minimum of the interaction by simple optimization method. Previous works derived the renormalization group equations by operator product expansion are especially useful in determine the low energy behavior of the interactions[9,21,22]. The couplings will eventually diverge with the constant ratio, which are independent of the initial values[9].

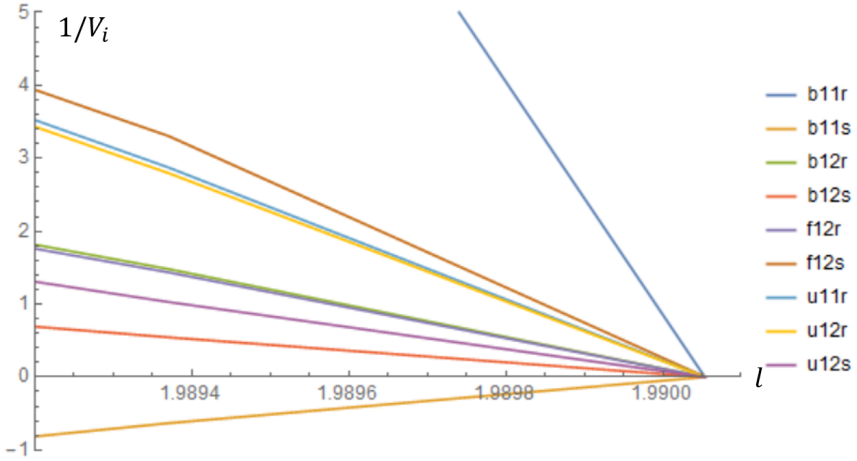

图 2-2: The flow of the nine independent couplings by simple RG.

As shown in Fig. 2-2, the plot shows the region just before the divergence. Apart from that $b_{11}^{\rho}, f_{12}^{\sigma}$ remain small, the inverses of the other couplings are "ray" like and,

$$b_{12}^{\rho} = \frac{1}{4} b_{12}^{\sigma} = f_{12}^{\rho} = -\frac{1}{4} b_{11}^{\sigma} = 2u_{11}^{\rho} = 2u_{12}^{\rho} = \frac{1}{2} u_{12}^{\sigma} = g > 0.$$

In the low energy effective action, the interaction term can be expressed as,

$$\mathcal{H}_{int} = -g(\psi_a^{\dagger} \tau^y \psi_a)^2,$$

where $\psi_a = (c_{Ra}, c_{La})$, τ^y is the y component of the Pauli matrices. Therefore, the effective Hamiltonian density becomes,

$$\mathcal{H} = i\psi_a^{\dagger} \tau^z \partial_x \psi_a - g(\psi_a^{\dagger} \tau^y \psi_a)^2,$$

where we redefine g and absorb v. The dirac fermion field can be expressed as two Majorana fields,

$$\psi_{Pa} = \frac{1}{\sqrt{2}} \left(\eta_{P2a} + i\eta_{P2a-1} \right).$$

The Hamiltonian density takes the standard form of SO(8) Gross-Neveu model,

$$\mathcal{H} = \frac{1}{2}\eta_{RA} i\partial_x \eta_{RA} - \frac{1}{2}\eta_{LA} i\partial_x \eta_{LA} + g G_R^{AB} G_L^{AB},$$

where the current G_P^{AB} is,

$$G_P^{AB} = i\eta_{PA}\eta_{PB}, A \neq B,$$

and $A, B = 1, ..., 8$. The 28 currents G_P^{AB} generate the chiral SO(8) transformation.

Renormalization group and its extension

Basic ideas of renormalization group

Renormalization group (RG) is a powerful method to find the low energy behavior of a non-linear model which has moderate coupling constant. In condensed matter physics, RG is very useful to investigate the diverse low energy phenomena emerge from the bare Coulomb interaction. The philosophy of such method is to treat each interaction with different energy scales, instead of treating them equally. One can step-by-step remove the high energy part and obtain the low energy effective action (LEEA) where the low energy phenomena emerge. Wilson first used the so-called Wilsonian renormalization group to investigate the critical phenomenon[23]. At each step of the Wilsonian renormalization group, the high energy part of the partition function is integrated out, the remaining low energy part is rescaled to the original one. Compared with the original parameters, one can derive the renormalization group flow equation. Different coupling constants behave variously when approaching the fixed point, there are relevant, marginal and irrelevant term for increasing, unchanged and decreasing coupling constant under the flow. Especially, some flow will end up with reaching fixed points which lead to a scale-invariant action.

When it comes to the fermion system, the ground state is redefined by the fermi level, the couplings cannot be reduced to a number with $d > 1$. They are coupling functions depend on the momenta and the corresponding flows are integro-differential equations. Shankar's famous review pedagogically presented the fermion version of the Wilsonian RG[17].

Patch functional renormalization group

is a specific version of Wilsonian RG. Polchinski developed the functional RG (FRG) to prove the renormalizability of the Φ^4 model in 4-dimension[24]. It turns out

to be a significant framework for computational purpose. The flow equations now describe the evolution of the generating functional for the vertex functions or many-body Green functions with the energy scale Λ[18]. FRG introduce the regulator to the bare Green functions which suppress the high energy part above the energy scale Λ. With the regularization, the flow for the functional can be viewed as the interpolation between the bare action and the low energy effective action. The flow is protected by Ward identity. Compared with the sharp cutoff in the original Wilsonian approach, the smooth regulator leads to an exact functional differential equation. More significantly, full information can be extracted from the flow instead of only the low energy part in the original Wilsonian RG. The name "functional renormalization group" comes from the flow for the generating functional. In this scheme, the momentum space is divided into *N* patches, we also call it *N*-patch FRG.

Singular-mode functional renormalization group

is a modified version of FRG. The vertex function in FRG method can be parameterized by a bilinear form which contains form factors with different channels, namely particle-particle channel, particle-hole crossing channel and particle-hole direct channel[19,20]. The five Feynman diagrams in FRG can be arranged into the three channels and yield the flow equations for each channel. We actually keep the important elements of the vertex function, which are more likely to diverge in the final stage. However, the channels have overlap on each other because when the particle scattering in a relative small region, different channels contribute to the same vertex function. When neglecting the channel overlaps, it corresponds to the random phase approximation. It is natural to combine the channels to give superconductivity, spin-density-wave and charge-density-wave. This method is what they dub "Singular mode functional renormalization group" or SMFRG[20].

In the following sections, we will introduce these methods and give applications on the two-leg ladder model.

Wilsonian renormalization group

General procedure

We will first formally derive the renormalization group and then apply it to the two-leg ladder model. We begin with the general Hamiltonian,

$$H = H_0 + H_{\text{int}},$$

where the free part, H_0, is a quadratic term and the interaction part, H_{int} is a quartic term. The corresponding partition function is,

$$Z = \int \prod_i [\mathcal{D}\bar{c}_i]\,[\mathcal{D}c_i] e^{-\sum_i S(\bar{c}_i, c_i)} = \int [\mathcal{D}\bar{c}_i]\,[\mathcal{D}c_i]\, e^{-S_0(\bar{c}_i, c_i) - S_{\text{int}}(\bar{c}_i, c_i)},$$

where S_0 is the free part action and S_{int} is the interaction part, we omit the sum symbol in the last expression. We now separate the fields c_i into fast mode and slow mode, which are defined as following,

$$c_i s = c_i(k), 0 \le k \le \Lambda/s,$$
$$c_i f = c_i(k), \Lambda/s \le k \le \Lambda,$$

where the cutoff Λ is largest momentum that allowed in our theory, or to say, our our theory is defined in the range $(0, \Lambda)$, $s > 1$ is a scale parameter. Now, the free part of the action can be separated into slow and fast piece, but the interaction part remain mixed,

$$\mathcal{Z} = \int [\mathcal{D}\bar{c}_i f]\,[\mathcal{D}c_i f]\,[\mathcal{D}\bar{c}_i s]\,[\mathcal{D}c_i s]\, e^{-S_0 f(\bar{c}_i f, c_i f) - S_0 s(\bar{c}_i s, c_i s) - S_{\text{int}}(\bar{c}_i f, c_i f, \bar{c}_i s, c_i s)}.$$

We now define the LEEA, S_{eff}, as,

$$\mathcal{Z} = \int [\mathcal{D}\bar{c}_i s]\,[\mathcal{D}c_i s] e^{-S_0(\bar{c}_i s, c_i s)} \int [\mathcal{D}\bar{c}_i f]\,[\mathcal{D}c_i f]\, e^{-S_0(\bar{c}_i f, c_i f) - S_{int}(\bar{c}_i s, c_i s, \bar{c}_i f, c_i f)},$$
$$\equiv \int [\mathcal{D}\bar{c}_i s]\,[\mathcal{D}c_i s] e^{-S_{eff}(\bar{c}_i s, c_i s)},$$

the LEEA can be expressed as,

$$
\begin{aligned}
e^{-S_{eff}(\bar{c}_i s, c_i s)} &= e^{-S_0(\bar{c}_i s, c_i s)} \int [D\bar{c}_i f]\,[Dc_i f]\, e^{-S_0(\bar{c}_i f, c_i f) - S_{int}(\bar{c}_i s, c_i s, \bar{c}_i f, c_i f)} \\
&= e^{-S_0(\bar{c}_i s, c_i s)} \frac{\int [D\bar{c}_i f][Dc_i f] e^{-S_0(\bar{c}_i f, c_i f) - S_{int}(\bar{c}_i s, c_i s, \bar{c}_i f, c_i f)}}{\int [D\bar{c}_i f][Dc_i f] e^{-S_0(\bar{c}_i f, c_i f)}} \int [D\bar{c}_i f]\,[Dc_i f]\, e^{-S_0(\bar{c}_i f, c_i f)} \\
&= e^{-S_0(\bar{c}_i s, c_i s)} \left\langle e^{-S_{int}(\bar{c}_i s, c_i s, \bar{c}_i f, c_i f)} \right\rangle_{S_0 f},
\end{aligned}
$$

where $\mathcal{Z}_0 = \int [\mathcal{D}\bar{c}_i f]\,[\mathcal{D}c_i f]\, e^{-S_0(\bar{c}_i f, c_i f)}$ is a constant and can be dropped without any influence on the LEEA. $\langle \ldots \rangle_{S_0 f}$ represents the average over free action of the fast modes.

Considering the expression for the mean of the exponential to the exponential of the means,

$$
\left\langle e^{\Omega} \right\rangle = e^{\langle \Omega \rangle + \frac{1}{2}\left(\langle \Omega^2 \rangle - \langle \Omega \rangle^2 \right) + \cdots}.
$$

The LEEA can be expressed as,

$$
S_{eff} = S_0 + \langle S_{int} \rangle - \frac{1}{2}\left(\left\langle S_{int}^2 \right\rangle - \langle S_{int} \rangle^2 \right) + \cdots .
$$

The term $\langle S_{int} \rangle$ gives tree-level contribution to the quartic interaction and one-loop correction to the quadratic term. Hence, after rescaling the momentum, frequency and fields, the LEEA can be compared with the bare action and give us the renormalization group equation. In this way the coupling constant as a function of cutoff can be obtained.

To see this, we consider a general form of the interaction action S_{int},

$$
\begin{aligned}
S_{\text{int}} = & \sum_{i,j,k,l} \int_{k\omega} (\bar{c}_i s + \bar{c}_i f)_4 (\bar{c}_j s + \bar{c}_j f)_3 (c_k s + c_k f)_2 (c_l s + c_l f)_1 \\
& u\,(4,3,2,1)\, \delta\,(k_1 + k_2 - k_3 - k_4)\, \delta\,(\omega_1 + \omega_2 - \omega_3 - \omega_4)\,,
\end{aligned}
$$

where i, j, k, l represent different band indices and spin indices, $1, 2, 3, 4$ are the abbreviation of the momentum k_i and frequency ω_i, the delta function imply the momentum conservation $k_1 + k_2 - k_3 - k_4 = 0$ and the frequency conservation.

Self energy correction

We first calculate the correction to the order u,

$$\left\langle \sum_{i,j,k,l} \int_{k\omega} (\bar{c}_i s + \bar{c}_i f)_4 (\bar{c}_j s + \bar{c}_j f)_3 (c_k s + c_k f)_2 (c_l s + c_l f)_1 \right.$$
$$\left. u\,(4,3,2,1)\,\delta\,(k_1 + k_2 - k_3 - k_4)\,\delta\,(\omega_1 + \omega_2 - \omega_3 - \omega_4) \right\rangle_{S_0 f},$$

when expanding the expression, there are 16 different monomials, but not all contribute finite value due to the symmetry. One can diagrammatically shows that the 16 different monomials actually can be classify into 4 different categories. Fig. 3–1 shows all the

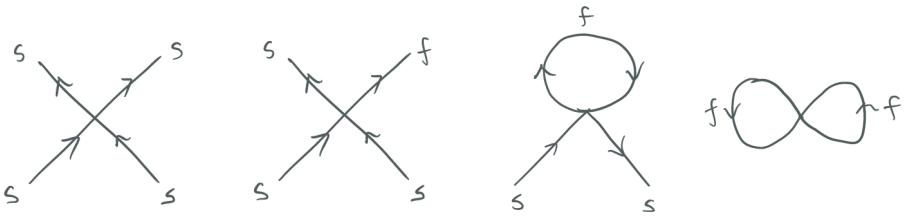

图 3–1: The Feynman diagrams for the renormalization.

4 different topological structures of the correction to the order u. The second one will vanish due to the symmetry and the forth one is a constant and have nothing to do with the LEEA. The first one is the tree-level contribution. The third graph contains two fast modes and two slow modes. Therefore, after eliminating the fast modes, this type of graph will contribute a correction to the quadratic interaction. The correction can be expressed as,

$$\delta\mu = u \int_{\Lambda/s<|k|<\Lambda} \frac{dk}{2\pi} G_0 f\left(0^+, k\right),$$

where $\delta\mu$ is the correction to the quadratic term, $G_0 f$ is the Green's function of the free part of the fast modes, 0^+ represents the time. For example, the Green's function of the linear dispersion is,

$$G_0 f\left(0^+, k\right) = \int_{-\infty}^{\infty} \frac{d\omega}{2\pi} e^{i\omega 0^+} \frac{1}{i\omega - vk}.$$

Interaction correction

To find the correction to the coupling constant, we need to calculate the u^2 order term, namely, $\langle S_{int}^2 \rangle - \langle S_{int} \rangle^2$. If we ignore the spin indices, there are 3 possible con-

nected diagrams will contribute while the disconnected diagrams cancel in the cumulant expansion. As shown in Fig. 3–2, we dub the diagrams ZS, ZS' and BCS respectively, they are just the labels for the topologies. The first two graphs will contribute equally to the coupling constant u while the last graph will pick up a factor $\frac{1}{2}$ due to the interchangeability of the internal lines. The loop frequencies in the ZS and ZS' graphs are equal, but those in the BCS graph are equal and opposite. The momentum transfer $Q = k_1 - k_3$ in the ZS graph, $Q' = k_1 - k_4$ in the ZS' graph, and $P = k_1 + k_2$ in the BCS graph.

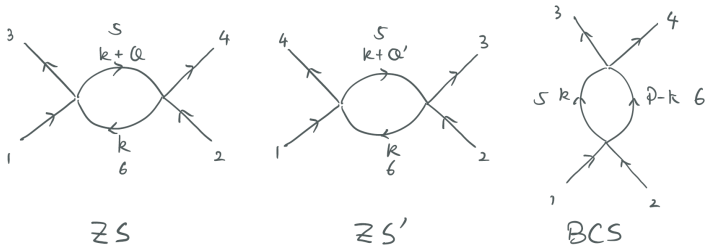

图 3–2: The Feynman diagrams for the renormalization.

The total correction to the interaction vertex is,

$$\begin{aligned} du\,(4321) &= \int u\,(6351)\,u\,(4526)\,G\,(5)\,G\,(6)\,\delta\,(3+6-1-5)d5d6 \\ &- \int u\,(6451)\,u\,(3526)\,G\,(5)\,G\,(6)\,\delta\,(4+6-1-5)d5d6 \\ &-\tfrac{1}{2}\int u\,(6521)\,u\,(4365)\,G\,(5)\,G\,(6)\,\delta\,(5+6-1-2)\,d5d6, \end{aligned}$$

where $1-6$ represent k_i, ω_i, the integration is integrate or sum over the momentum, the frequency and the band indices.

Applying to two-leg ladder model

We now apply the simple renormalization group method to the two-leg ladder model. The action of the free part is,

$$S_0 = \sum_{\alpha,i=L,R} \int_{-\Lambda}^{\Lambda} \frac{dk_{1,2}}{2\pi} \int \frac{d\omega}{2\pi} \{(-i\omega + vk_1)\,\bar{c}_{1i,\alpha} c_{1i,\alpha} + (-i\omega + vk_2)\,\bar{c}_{2i,\alpha} c_{2i,\alpha}\}, \quad (3\text{–}1)$$

where $k_1 = |K| - K_{F1}, k_2 = |K| - K_{F2}$. Because we only consider the flow of the quartic terms, the chemical potential is neglected. As shown in Fig. 3-3, the Brillouin zone

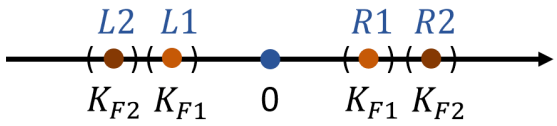

图 3-3: The labels for different momentum regions.

is divided into 4 regions, labeled by L_2, L_1, R_1, R_2 and corresponding Fermi momenta respectively. When momentum k lies in one of these regions, we simply assign the momentum with the label and corresponding Fermi momentum. The general form of the two particle (quartic) interaction can be expressed as,

$$\begin{aligned}\delta S_{int} = & \sum_{i,j,k,l=R_1,R_2,L_1,L_2} \sum_{\alpha,\beta,\gamma,\delta=\uparrow\downarrow} \int \frac{dk}{2\pi}\frac{d\omega}{2\pi} \bar{c}_{i\alpha}(k_4)\, \bar{c}_{j\beta}(k_3)\, c_{k\gamma}(k_2)\, c_{l\delta}(k_1) \\ & u_{\alpha,\beta,\gamma,\delta}(k_4,k_3,k_2,k_1)\, \delta(k_1+k_2-k_3-k_4)\, \delta(\omega_1+\omega_2-\omega_3-\omega_4),\end{aligned} \tag{3-2}$$

where $k_i = L_1, L_2, R_1, R_2$. We first neglect the spin indices. As shown in Fig. 3-4 These quartic interactions can be classified into forward, backward and umklapp scattering. For example, $u(L_1, L_1, L_1, L_1), u(R_2, L_1, R_1, L_2)$ are the forward scattering, $u(L_2, R_1, R_1, L_2)$, $u(L_1, R_1, R_2, L_2)$ are the backward scattering and $u(R_2, R_1, L_1, L_2)$ is the umklapp scattering.

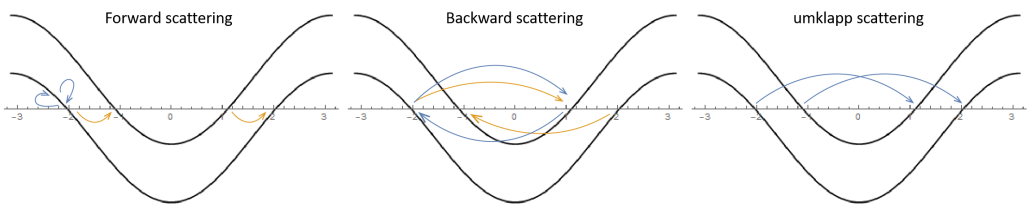

图 3-4: Different two particle scattering. The arrows with the same color correspond to the same process.

The partition function for this model is,

$$
\begin{aligned}
Z &= \int \prod_{i=1,2} \left[\mathcal{D}\bar{c}_i\right]\left[\mathcal{D}c_i\right] e^{-\sum_i S\left(\bar{c}_i, c_i\right)} \\
S &= \sum_{i=L,R} \int_{-\Lambda}^{\Lambda} \frac{dk_{1,2}}{2\pi} \int \frac{d\omega}{2\pi} \left\{\left(-i\omega + vk_1\right)\bar{c}_{1i}c_{1i} + \left(-i\omega + vk_2\right)\bar{c}_{2i}c_{2i}\right\} \\
&+ \sum_{i,j,k,l=R_1,R_2,L_1,L_2} \int \frac{dk}{2\pi}\frac{d\omega}{2\pi} \bar{c}_i\left(k_4\right)\bar{c}_j\left(k_3\right)c_k\left(k_2\right)c_l\left(k_1\right)u\left(k_4,k_3,k_2,k_1\right)\delta\left(\sum k_m\right)\delta\left(\sum \omega_m\right).
\end{aligned}
$$

We mainly focus on the correction to the interaction vertex. Following the previous procedure, the fields are separated into fast modes and slow modes, then we integrate out the fast modes and leave the LEEA. After rescaling the momenta, frequencies and the fields, we can compare the LEEA with the bare action and find the renormalization group correction to the coupling constants. Using,

$$
\begin{aligned}
&\xi_i(-k) = \xi_i(k) \\
&\xi_1(k \pm \pi) = -\xi_2(k) \\
&\xi_2(k \pm \pi) = -\xi_1(k),
\end{aligned}
\tag{3-3}
$$

leads to, for example, the forward scattering $u(R_2, L_1, R_1, L_2)$ only have ZS and BCS graphs, the momentum transfers are,

$$
\begin{aligned}
Q &= k_1 - k_3 = K_{F1} - K_{F2} \\
P &= k_1 + k_2 = K_{F1} - K_{F2},
\end{aligned}
$$

and the renormalization part du is,

$$
\begin{aligned}
&du(R_2, L_1, R_1, L_2) = \\
&+4 \times \int \frac{d\omega}{2\pi} \sum_k u(k+Q, L_1, k, L_2) u(R_2, k, R_1, k+Q) G_1\left(\omega, k\right) G_2\left(\omega, k+Q\right) \\
&-2 \times \Big(\int \frac{d\omega}{2\pi} \sum_k u(k+Q', R_1, k, R_2) u(L_1, k, L_2, k+Q') G_1\left(\omega, k\right) G_1\left(\omega, k+Q'\right) \\
&+ \int \frac{d\omega}{2\pi} \sum_k u(k+Q', R_1, k, R_2) u(L_1, k, L_2, k+Q') G_2\left(\omega, k\right) G_2\left(\omega, k+Q'\right)\Big) \\
&-4 \times \frac{1}{2} \int \frac{d\omega}{2\pi} \sum_k u(P-k, k, R_1, L_2) u(R_2, L_1, P-k, k) G_1\left(\omega, k\right) G_2\left(-\omega, P-k\right).
\end{aligned}
$$

Other scattering process can be calculated in the similar way. Hence, we can tabulate the coupling constants dependent on the 4 momentum points. Without the consid-

eration of the symmetry, at each step we have to calculate $4^3 = 64$ coupling constants. Therefore, we obtain the renormalization group flows for the coupling constants by multiplying *du* by the step length of the energy scale and add to *u*.

Functional renormalization group

Wilsonian renormalization group method offers deep and rigorous understanding of the interacting fermion system. An alternative way to apply the Wilsonian renormalization group is the exact renormalization group equations (ERGE) or functional renormalization group. The ERGE describes the evolution of the generating functional and can be viewed as an interpolation between the bare action and the low energy effective action of the system. Meanwhile, the ERGE contains not only the low energy information, full information can be extracted from the flow.

Useful functionals

To formulate the ERGE, we should first introduce some generating functionals to facilitate our description. We begin with the general two-particle interaction action,

$$\mathcal{S}[\psi,\bar{\psi}] = -\left(\bar{\psi}, G_0^{-1}\psi\right) + V[\psi,\bar{\psi}],$$

where $\psi, \bar{\psi}$ are Grassmann fields for fermion, G_0 is the bare Green's function,

$$G_0(x,x') = \delta_{\omega,\omega'}\delta_{k,k'}\delta_{\sigma,\sigma'}\frac{1}{i\omega - \xi_0(k)},$$

$V[\psi,\bar{\psi}]$ is an arbitrary two-particle interaction,

$$V[\psi,\bar{\psi}] = \frac{1}{4}\sum_{\substack{x_1,x_2\\y_1,y_2}} V(y_1,y_2;x_1,x_2)\,\bar{\psi}(y_1)\,\bar{\psi}(y_2)\,\psi(x_2)\,\psi(x_1),$$

where x_1, x_2, y_1, y_2 are general indices for the particles, for example Matsubara frequency, momentum, spin and sublattice indices. We omit the pre-factor which is dependent on the volume of the system or the temperature.

We now define the generating functional, in which the connected Green function can be obtained,

$$\mathcal{G}[\eta,\bar{\eta}] = -\ln\int \mathcal{D}\psi\mathcal{D}\bar{\psi}e^{-\mathcal{S}[\psi,\bar{\psi}]}e^{(\bar{\eta},\psi)+(\bar{\psi},\eta)},$$

where η is the source term. The connected $m-$particle Green functions are given by,

$$G^{(2m)}(x_1,...,x_m;x_1{}',...,x_m{}') = (-1)^m\frac{\partial^{2m}\mathcal{G}[\eta,\bar{\eta}]}{\partial\bar{\eta}(x_1)...\partial\bar{\eta}(x_m)\partial\eta(x_m{}')...\partial\eta(x_1{}')}|_{\eta,\bar{\eta}=0}.$$

ERGEs are more conveniently formulated by using the Legendre transform of the generating functional $\mathcal{G}[\eta,\bar{\eta}]$,

$$\Gamma[\psi,\bar{\psi}] = (\bar{\eta},\psi)+(\psi,\eta)+\mathcal{G}[\eta,\bar{\eta}],$$

Γ is so-called effective action which can generate the irreducible vertex functions.

$$\Gamma^{(2m)}(x_1{}',...,x_m{}';x_1,...,x_m) = \frac{\partial^{2m}\Gamma[\eta,\bar{\eta}]}{\partial\bar{\psi}(x_1{}')...\partial\bar{\psi}(x_m{}')\partial\psi(x_m)...\partial\psi(x_1)}|_{\psi,\bar{\psi}=0}.$$

The relation between generating function $\mathcal{G}$ and effective action Γ gives the general relation between the connected Green function and the irreducible vertex function,

$$\begin{aligned}
&\Gamma^{(2)} = G^{-1}\\
&G^{(4)}(12;34) = \sum_{56,78} G(1,7)\,G(2,8)\,\Gamma^{(4)}(78;56)\,G(5,3)\,G(6,4)\\
&G^{(6)} = G^3\Gamma^{(6)}G^3 + G^3\Gamma^{(4)}G\Gamma^{(4)}G^3.
\end{aligned}$$

To derive the ERGEs, another useful functional, effective interaction, should be introduced, however, we don't want to present the detailed derivation which can be found in reference[18]. The first three renormalization group equations are shown in Fig. 3–5. In the equations, the G^Λ is the full propagator, defined as, $\left(G^\Lambda\right)^{-1} = \left(G_0^\Lambda\right)^{-1} - \Sigma^\Lambda$. The Σ^Λ is the self energy and $S^\Lambda = \frac{d}{d\Lambda}G^\Lambda|_{\Sigma^\Lambda fixed}$

Although the ERGEs are non-perturbative, the flow equation for $2m$ order irreducible vertex function will contain $2m+2$ order irreducible vertex function. Hence, for simplicity, we make the truncation at 4th order and set $\Gamma^{(2m)} = 0$ for $m > 2$ in the calculation. Meanwhile, the self energy correction is neglected in the calculation.

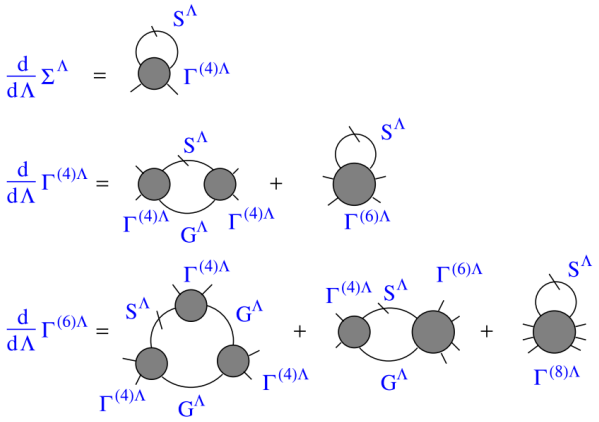

图 3–5: The diagrammatic representation of the flow equations for self energy, two-particle vertex function and three-particle vertex function. The slash on the internal lines means the Λ derivative of the Green function.

Therefore, diagrammatically, we focus on the equation,

$$\frac{d}{d\Lambda}\Gamma^{(4)\Lambda} = \Gamma^{(4)\Lambda} G^{\Lambda} S^{\Lambda} \Gamma^{(4)\Lambda}$$

Regulator

The significant improvement of ERGE is to introduce the regulator to the bare Green function. In a translation invariance system, one can introduce the regulator to the momentum,

$$G_0^{\Lambda} = \frac{\theta^{\Lambda}(k)}{i\omega - \xi_k},$$

where Λ is the cutoff, the regulator θ^{Λ} should vanish when $\xi_k \ll \Lambda$ and be equal to 1 when $\xi_k \gg \Lambda$. For simplicity, we introduce the Heaviside theta function to the bare Green function,

$$\theta^{\Lambda}(k) = \Theta\left(|\xi_k| - \Lambda\right).$$

The derivative of Heaviside theta function is delta function and easy to be integrated out. The momentum cutoff does not destroy the analytical properties of the propagators and vertex functions in the complex plane, and the Matsubara frequency can be analytically sum up.

When doing numerical calculation, we would like to use frequency regulator,

$$\vartheta\left(|\omega|/\Lambda\right),$$

where $\vartheta(x)$ vanishes for $x \ll 1$ and tends to 1 for $x \gg 1$. Contrast to the momentum cutoff regulator, the frequency one has several advantages, it will not interfere with Fermi surface shifts, particle-hole processes with small momentum transfers are captured smoothly by the flow, and it can be used in systems without translational invariance. Therefore, the cutoff dependent Green function is,

$$G_0^{\Lambda} = \frac{\theta\left(|\omega| - \Lambda\right)}{i\omega - \xi_k}, S^{\Lambda} = \frac{\delta\left(|\omega| - \Lambda\right)}{i\omega - \xi_k}.$$

SU(2) invariant system

As a consequence of the spin rotation symmetry, the two-particle vertex with spin indices s_i and multi-index K_i can be expressed as,

$$\begin{aligned}&\Gamma^{(4)\Lambda}_{s_1 s_2 s_3 s_4}\left(K_1, K_2; K_3, K_4\right) = \\ &V^{\Lambda}\left(K_1, K_2; K_3, K_4\right)\delta_{s_1,s_3}\delta_{s_2,s_4} - V^{\Lambda}\left(K_2, K_1; K_3, K_4\right)\delta_{s_1,s_4}\delta_{s_2,s_3},\end{aligned} \tag{3-4}$$

where the multi-index contains frequency, momentum and band index. The flow equation for the coupling function is,

$$\frac{d}{d\Lambda}V^{\Lambda} = \mathcal{T}^{\Lambda}_{PP} + \mathcal{T}^{\Lambda}_{PH,d} + \mathcal{T}^{\Lambda}_{PH,cr}, \tag{3-5}$$

where $\mathcal{T}_{PP}$ represents the particle-particle channel, $\mathcal{T}_{PH,d}$ and $\mathcal{T}_{PH,cr}$ represent the direct and crossing particle-hole channel respectively.

$$\begin{aligned}&T^{\Lambda}_{PP}\left(K_1, K_2; K_3, K_4\right) = \\ &\int dK \times V^{\Lambda}\left(K_1, K_2, K\right) L^{\Lambda}\left(K, -K + K_1 + K_2\right) V^{\Lambda}\left(K, -K + K_1 + K_2, K_3\right),\end{aligned} \tag{3-6}$$

$$
\begin{aligned}
&T^{\Lambda}_{PH,d}\left(K_1,K_2;K_3,K_4\right)= \\
&\int dK[-2V^{\Lambda}\left(K_1,K,K_3\right)L^{\Lambda}\left(K,K+K_1-K_3\right)V^{\Lambda}\left(K+K_1-K_3,K_2,K\right) \\
&+V^{\Lambda}\left(K_1,K,K+K_1-K_3\right)L^{\Lambda}\left(K,K+K_1-K_3\right)V^{\Lambda}\left(K+K_1-K_3,K_2,K\right) \\
&+V^{\Lambda}\left(K_1,K,K_3\right)L^{\Lambda}\left(K,K+K_1-K_3\right)V^{\Lambda}\left(K_2,K+K_1-K_3,K\right)],
\end{aligned}
\tag{3-7}
$$

$$
\begin{aligned}
&T^{\Lambda}_{PH,cr}\left(K_1,K_2;K_3,K_4\right)= \\
&\int dK\times V^{\Lambda}\left(K_1,K+K_2-K_3,K\right)L^{\Lambda}\left(K,K+K_2-K_3\right)V^{\Lambda}\left(K,K_2,K_3\right),
\end{aligned}
\tag{3-8}
$$

where $L^{\Lambda}\left(K,K'\right)=S^{\Lambda}\left(K\right)G^{\Lambda}\left(K'\right)+G^{\Lambda}\left(K\right)S^{\Lambda}\left(K'\right)$. The corresponding Feynman diagrams are shown in Fig. 3-6.

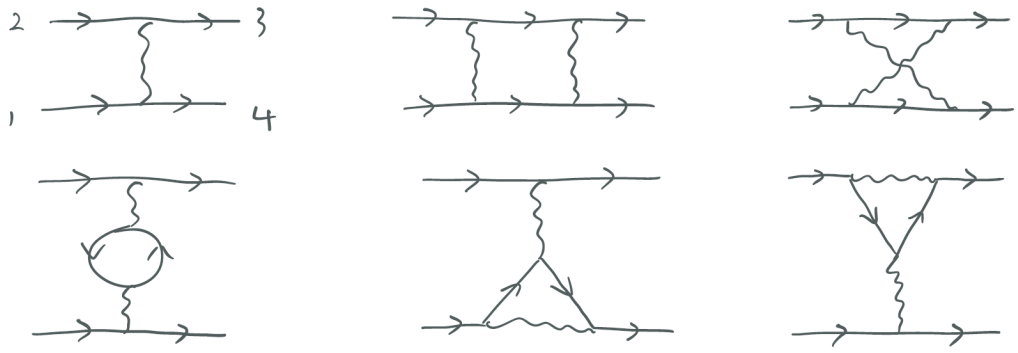

图 3-6: The Feynman diagrams for the SU(2) invariant system.

Singular-mode functional renormalization group

As shown in Fig. 3-7, the vertex function can be parameterized into specific channels, namely Pairing, Crossing, Direct. We use the first letter to label the channels,

$$
\begin{aligned}
&\Gamma^{abcd}_{k+q,-k,-p,p+q}\rightarrow\sum_{mn}f^{ab*}_{m}(k)P^{ab;cd}_{mn}(q)f^{cd}_{n}(p) \\
&\Gamma^{abcd}_{k+q,p,k,p+q}\rightarrow\sum_{mn}f^{ac*}_{m}(k)C^{ac;bd}_{mn}(q)f^{bd}_{n}(p) \\
&\Gamma^{abcd}_{k+q,p,p+q,k}\rightarrow\sum_{mn}f^{ad*}_{m}(k)D^{ad;bc}_{mn}(q)f^{bc}_{n}(p),
\end{aligned}
$$

where a,b,c,d are the band indices and spin indices, k,p,q are the momentum, f^{ab}_{m} is the form factor. This parameterization can be seen from the Fourier transformation of

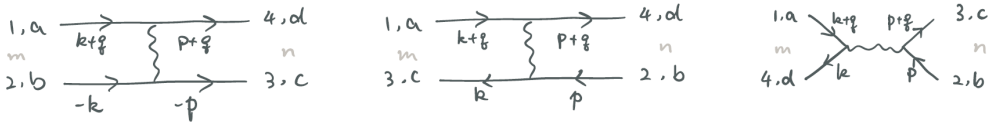

图 3–7: The Feynman diagrams for the P, C, D channels, a, b, c, d represents the sublattice indices or spin indices.

the real space vertex function, for example, the P channel, the interaction action is,

$$V = \sum_{r_0,r,r',R} \sum_{abcd} c_a^\dagger(r_0) c_b^\dagger(r_0 + r) c_c(r_0 + R + r') c_d(r_0 + R) P^{abcd}(r_0, r, r', R),$$

where $c_i^\dagger, c_i$ are the creation and annihilation operators with band index i. Because of the translational invariance, we can set $r_0 = 0$, the parameterization is now dependent on the relative distance of the incoming and outgoing particles, r, r', and their separation R. Considering the Fourier transformation Eq. 2–3, in momentum space, the interaction action is,

$$\begin{aligned} V = &\sum_{k,p,q} \sum_{r,r',R} \sum_{abcd} c_a^\dagger(k+q) e^{-i(k+q)(0)} c_b^\dagger(-k) e^{-i(-k)(r)} \\ &c_c(-p) e^{i(-p)(R+r')} c_d(p+q) e^{i(p+q)(R)} P^{abcd}(r, r', R). \end{aligned} \tag{3–9}$$

The real space channel is parameterized as,

$$P^{ab;cd}(r, r', R) = \sum_{mn} f_m^{ab}(r) P_{mn}^{ab;cd}(R) f_n^{cd}(r'), \tag{3–10}$$

where $f_m^{ab}(r)$ is the form factor m of band a, b with relative position r, for example, $f_m^{ab}(r) = 1$ when $a = b, r = 0$ for the on-site, $a = b, r = \pm 1$ for the nearest neighbour and $a \neq b, r = 0$ for the hopping between two bands. We assume in real space only the particles in short distance will scatter, adding the next-nearest neighbour will not change our results. Hence, it confirms our previous assumption. In this case, the form factor forms a 8-vector, because # of on-site and nearest neighbours = 4 times the # of sublattice = 2. Plug Eq. 3–10 into Eq. 3–9, the Fourier transformation factor can be absorbed into the expression of the channel, therefore we define,

$$\sum_{mn} \sum_{r,r',R} e^{ikr} f_m^{ab}(r) \times e^{iqR} P_{mn}^{ab;cd}(R) \times e^{-ipr'} f_n^{cd}(r') \equiv \sum_{mn} f_m^{ab}(k) P_{mn}^{ab;cd}(q) f_n^{cd*}(p), \tag{3–11}$$

the form factors in real space are delta function, thus they have simple form in the momentum space. Similar to the previous method, we want to investigate the 1-loop correction to the vertex functions. In this parameterization, the 1-loop contribution to

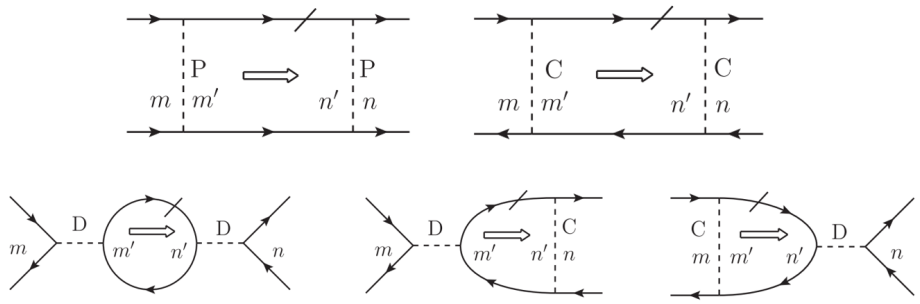

图 3-8: The Feynman diagrams for the 1-loop corrections to the P, C, D channels.

each channel has two parts, the channel itself, $\partial P, \partial C, \partial D$, and the projection of other channels. The Feynman diagrams for the corrections are shown in Fig. 3-8. The expression for $\partial P, \partial C, \partial D$ can be written as a matrix product form,

$$\begin{aligned}
\partial P/\partial\Lambda &= P\chi_{pp}{}'P, \\
\partial C/\partial\Lambda &= C\chi_{ph}{}'C, \\
\partial D/\partial\Lambda &= (C-D)\chi_{ph}{}'D + D\chi_{ph}{}'(C-D),
\end{aligned}$$

where the particle-particle bubble χ_{pp} and particle-hole bubble χ_{ph} are calculated by,

$$\begin{aligned}
&(\chi_{pp}{}')^{a'b'c'd'}_{m'n'} = \tfrac{\partial}{\partial\Lambda}\int\tfrac{d\omega}{2\pi}\int\tfrac{dp}{2\pi} f^{a'b'}_{m'}(p) G^{a'd'}(p+q,i\omega)\, G^{b'c'}(-p,-i\omega)\, f^{c'd'*}_{n'}(p)\theta(|\omega|-\Lambda) \\
&= -\tfrac{1}{2\pi}\int\tfrac{dp}{2\pi} f^{a'b'}_{m'}(p) G^{a'd'}(p+q,i\Lambda)\, G^{b'c'}(-p,-i\Lambda)\, f^{c'd'*}_{n'}(p) + (\Lambda\to-\Lambda)
\end{aligned}$$

$$\begin{aligned}
&(\chi_{ph}{}')^{a'b'c'd'}_{m'n'} = \tfrac{\partial}{\partial\Lambda}\int\tfrac{d\omega}{2\pi}\int\tfrac{dp}{2\pi} f^{a'b'}_{m'}(p) G^{a'd'}(p+q,i\omega)\, G^{b'c'}(p,i\omega)\, f^{c'd'*}_{n'}(p)\theta(|\omega|-\Lambda) \\
&= -\tfrac{1}{2\pi}\int\tfrac{dp}{2\pi} f^{a'b'}_{m'}(p) G^{a'd'}(p+q,i\Lambda)\, G^{b'c'}(p,i\Lambda)\, f^{c'd'*}_{n'}(p) + (\Lambda\to-\Lambda),
\end{aligned}$$

where the Green functions are in sublattice representation but not band representation,

$$G^{-1}(\omega,k) = i\omega\mathbb{I}_2 - \begin{pmatrix} -2t\cos k & -t_\perp \\ -t_\perp & -2t\cos k \end{pmatrix}, \tag{3-12}$$

where $\mathbb{I}_2$ represents $2d$ identity matrix. However, other channels will also contribute,

by projecting other channels, the total increasement of each channel is,

$$\begin{aligned}
\frac{dP}{d\Lambda} &= \frac{\partial P}{\partial \Lambda} + \hat{P}(\frac{\partial C}{\partial \Lambda} + \frac{\partial D}{\partial \Lambda}) \\
\frac{dC}{d\Lambda} &= \frac{\partial C}{\partial \Lambda} + \hat{C}(\frac{\partial P}{\partial \Lambda} + \frac{\partial D}{\partial \Lambda}) \\
\frac{dD}{d\Lambda} &= \frac{\partial D}{\partial \Lambda} + \hat{D}(\frac{\partial P}{\partial \Lambda} + \frac{\partial C}{\partial \Lambda}),
\end{aligned}$$

where the operator $\hat{P}$ means projecting other channels into the P channel.

Projection of channels

From the real space vertex function, we can find that other channels contribute to the same graph, we can arrange the diagrams of P, C, D channel to the typical one,

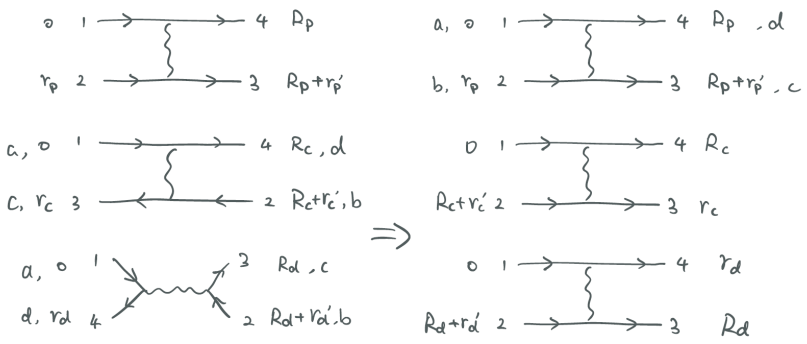

图 3–9: The rearrangement of the C, D channels and map them to P channel.

As shown in Fig. 3–9, if $|R_c + r'_c - r_p| < \delta, |R_c - R_p| < \delta, |r_c - (R_p + r'_p)| < \delta$ then the channel $C(r_c, r'_c, R_c)$ are allowed to map to channel $P(r_p, r'_p, R_p)$. The δ is the cutoff, we choose $\delta = 10^{-5}$ in our calculation. Similarly, if $|R_d + r'_d - r_p| < \delta, |r_d - R_p| < \delta, |R_d - (R_p + r'_p)| < \delta$ then the channel $D(r_d, r'_d, R_d)$ can be mapped to channel $P(r_p, r'_p, R_p)$. Other projection of channel can be done in the similar way.

The flow equation works in the momentum space, therefore, we have to Fourier transform each channel. By definition in Eq. 3–11, the Fourier transformation of the P channel in momentum space is,

$$P^{ab;cd}_{mn}(R) = \sum_q P^{ab;cd}_{mn}(q) e^{-iqR}, \tag{3–13}$$

C, D channel can be Fourier transformed in the similar way. The total vertex function

for P type channel is thus,

$$\begin{aligned}\Gamma^{ab;cd}(r,r',R) &= \sum_{mn} f_m^{ab}(r) P_{mn}^{ab;cd}(R) f_n^{cd}(r') \\ &+ \sum_{mn} f_m^{ac}(r) C_{mn}^{ac;bd}(R_c(r,r',R)) f_n^{bd}(r') \\ &+ \sum_{mn} f_m^{ad}(r) D_{mn}^{ad;bc}(R_d(r,r',R)) f_n^{bc}(r'),\end{aligned} \tag{3-14}$$

where $R_c(r,r',R), R_d(r,r',R)$ are allowed mapping from C, D channel to P channel. P channel with the projection of other channels can be recovered by,

$$\widetilde{P}_{mn}^{ab;cd}(R) = \sum_{r,r'} f_m^{ab}(r) \Gamma^{ab;cd}(r,r',R) f_n^{cd}(r'). \tag{3-15}$$

Finally, we take the Fourier transformation and obtain the total correction to the P channel with mixing other channels, $\widetilde{P}_{mn}^{abcd}(q)$.

$$\widetilde{P}_{mn}^{ab;cd}(q) = \sum_{R} \widetilde{P}_{mn}^{ab;cd}(q) e^{iqR}. \tag{3-16}$$

Numerical calculation and results

In this chapter, we present the numerical implementation and the results of applying FRG and SMFRG on two-leg ladder model. Although the model is quasi-1d, it contains two bands and the implementation can be easily generalized to higher dimension with multi-band. It is promising to investigate the cuprate, iron-based superconductors and other strong correlated system.

N-patch functional renormalization group

In this section, we present the detailed implementation and results obtained by functional renormalization group method, namely, numerically calculate Eq. 3-5. The momentum space, which is a segment $[-\pi, \pi]$, is divided into several non-uniform patches. From the bare Green function $G(\omega, k) = \frac{1}{i\omega - \xi(k)}$, only the momentum close to the Fermi momentum will largely contribute. We set the patches near the Fermi momentum, for example, we divide the segment $[k_{F1} - dk, k_{F1} + dk]$ into $N/4$ patches. Based on the division, the discrete version of the band structure can be constructed with the patch index $i \in [1, N]$.

We also need to impose momentum conservation in our calculation,

$$\bar{\delta}\left(k_1 + k_2 - k_3 - k_4\right) \Leftrightarrow \left(k_1 + k_2 - k_3 - k_4\right) \bmod 2\pi = 0.$$

The momentum k_4 can be determined by k_1, k_2, k_3. In each step, the 1-loop integration Eq. 3-6, Eq. 3-7 and Eq. 3-8 are calculated numerically. The expression for $L^{\Lambda}(K, K')$ is,

$$L^{\Lambda}\left(K, K'\right) = \frac{1}{2\pi} \int_{-r}^{r} \frac{1}{i\Lambda - E\left(K\right)} \frac{1}{i\Lambda - E\left(K'\right)} + h.c.,$$

where r is the cutoff of the momentum. For the linearized band structure, $E(K) =$

$E_0 + vK$, the integration can be carried out analytically. We label the function for the linearized band as $L_0^{\Lambda}(\Lambda, E_1, v_1, E_2, v_2)$, where E_1, E_2 are the energies at K, K' and v_1, v_2 are the velocity at K, K'. The bubble for particle-particle channel and particle hole channel are,

$$\chi_{pp}^{\Lambda}(k_5, k_6) = -L_0^{\Lambda}(\Lambda, E(k_5), v(k_5), -E(k_6), v(k_6))$$
$$\chi_{ph}^{\Lambda}(k_5, k_6) = L_0^{\Lambda}(\Lambda, E(k_5), v(k_5), E(k_6), v(k_6)).$$

Till now, we can calculate the increasement of each 1-loop diagram in Fig. 3–6. For specific k_1, k_2, k_3, we first check whether $k_4(k_1, k_2, k_3)$ exist, then loop the internal momentum k_5, k_6. k_6 is dependent on k_5 and other external momenta, for example, the python code is,

```
#particle-particle channel
if k6[k1,k2,k5] != -1:
dG[k1,k2,k3] = dG[k1,k2,k3] + G[k1,k2,k5] * xpp[k5,k6] *
    G[k6,k5,k3]

#particle-hole cross channel
if k6[k1,k5,k3] != -1:
dG[k1,k2,k3] = dG[k1,k2,k3] + G[k1,k5,k3] * xph[k5,k6] *
    G[k6,k2,k5]

#particle-hole direct channel
if k6[k5,k2,k3] != -1:
dG[k1,k2,k3] = dG[k1,k2,k3] - 2 * G[k1,k6,k5] * xph[k5,k6] *
    G[k5,k2,k3]
if k6[k5,k2,k3] != -1:
dG[k1,k2,k3] = dG[k1,k2,k3] + G[k1,k6,k4] * xph[k5,k6] *
    G[k5,k2,k3]
if k6[k2,k5,k3] != -1:
dG[k1,k2,k3] = dG[k1,k2,k3] + G[k1,k6,k5] * xph[k5,k6] *
    G[k2,k5,k3]
```

In this code, -1 stands for that the momentum is not allowed by the conservation law.

Next step is to combine the single steps. We define the ultraviolet cutoff and the infrared cutoff and decrease the frequency cutoff Λ from UV cutoff to IR cutoff in each cycle. However, the order parameter will diverge before Λ goes to IR cutoff.

Singular-mode renormalization group method

We first present the setups of the implementation. Singular mode renormalization group requires properly choice of the form factor to parameterize each channel. The form factors we chose here have on-site and nearest neighbour,

$$f_m^{ab}(r) = [\delta_{ab}\delta_{r,0}, \delta_{ab}\delta_{r,-1}, \delta_{ab}\delta_{r,1}, (1-\delta_{ab})\delta_{r,0}],$$

where the elements in the vector corresponds to $m = 1, 2, 3, 4$. When taking the Fourier transformation,

$$f_m^{ab}(k) = [\delta_{ab}, \delta_{ab}e^{-ik}, \delta_{ab}e^{ik}, (1-\delta_{ab})].$$

As defined in Eq. 3-12, the Green function depends on the sublattice indices, we label it by $G^{ab}(\omega, k)$. We also need the matrix for the channels in real and momentum space, they are labeled by, say, $P(q, a, b, m; c, d, n)$, $P(R, a, b, m; c, d, n)$. The index $a, b, m; c, d, n$ can be bound up and the matrix can be reshaped into $P(q, m, n)$, $P(R, m, n)$, here, $(a, b, m) \to m$, $(c, d, n) \to n$. The reshaped matrices will facilitate our calculation.

In each step, the skeleton of the calculation is,

```
#Caluclate the bubbles, xpp(q,a,b,m,c,d,n)
for q in range(nq):
for a in range(nsublattice):
...
xpp[q,a,b,m,c,d,n] = xpp_int(Lc,qrange[q],m,n,a,b,c,d)
xph[q,a,b,m,c,d,n] = xph_int(Lc,qrange[q],m,n,a,b,c,d)
#reshape into the multi-index form
xpp = xpp.reshape(xpp,(nq,N,N))
xph = xph.reshape(xph,(nq,N,N))
```

```
#Increasement in each channel
dPchannel, dCchannel, dDchannel =
    np.zeros((nq,N,N)),np.zeros((nq,N,N)),np.zeros((nq,N,N))

for q in range(nq):
dPchannel[q] = np.dot(np.dot(Pchannel[q],xpp[q]),Pchannel[q])
dCchannel[q] = np.dot(np.dot(Cchannel[q],xph[q]),Cchannel[q])
dDchannel[q] = np.dot(np.dot((Cchannel[q] -
    Dchannel[q]),xph[q]),Dchannel[q])\
+ np.dot(np.dot(Dchannel[q],xph[q]),(Cchannel[q] - Dchannel[q]))

#mapping channel, we do the mapping in real space, we first need
    to Fourier transform them into real space, say, dPchannelR,
    we also need to define the mixed channel, say,
    dPchannelR_mixed

FourierTrans(dPchannel, dCchannel, dDchannel)

dPchannelR_mixed, dCchannelR_mixed, dDchannelR_mixed =
    dPchannelR, dCchannelR, dDchannelR

#project the single channel into the mixed one
proj(dPchannelR, dCchannelR, dDchannelR, dPchannelR_mixed,
    dCchannelR_mixed, dDchannelR_mixed)

#Inverse Fourier transform dPchannelR_mixed to the original
    dPchannel
InvFourierTrans(dPchannelR_mixed, dCchannelR_mixed,
    dDchannelR_mixed)

#Finnaly,
Pchannel = np.add(Pchannel, dPchannel)
Cchannel = np.add(Cchannel, dCchannel)
```

```
Dchannel = np.add(Dchannel, dDchannel)
```

In the calculation, the form factor can be labelled by 1 sublattice index, instead of $f_m^{ab}(r)$. Because the position vector r can identify the sublattice. For example, r could be on-site and nearest neighbours in the single chain and one nearest neighbour on the other chain. In this representation, all the elements in the form factors, channels and bubbles are non-zero. However, for 2 sublattices system, in the naive representation, $f_m^{ab}(r)$, not all the form factors are legal, therefore, one has to carefully set specific elements to be zero. For instance, when $a \neq b$, r cannot be $-1, 1$, the corresponding form factors are 0. A simple method is to tabulate the elements as,

$$P_{mn}^{ab;cd}(R) = \sum_{r,r'} f_m^{ab}(r) \left(\sum_{s,t} f_s^{ab}(r) P_{st}^{ab;cd}(R) f_t^{cd}(r') \right) f_n^{cd}(r').$$

Results and analysis of the data from FRG

In the FRG method, we obtain the vertex functions with discrete momentum indices. However, it is not straightforward to compare the vertex functions with other results. Here, we arrange the vertex functions into different representations, which will facilitate our analysis.

Arrange the vertex functions into channels

The discrete momenta can be grouped to represent possible channels, namely, pair-density-wave, spin-density-wave and charge-density-wave. All the k_1, k_2, k_3, k_4 which satisfy $k_1 + k_2 - q_{sc} \mod 2\pi = 0$ and $k_3 + k_4 - q_{sc} \mod 2\pi = 0$ will contribute to the pair-density-wave channel, where $q_{sc} = 0$. Hence, define $V(k_1, k_4) = \sum_{k_2,k_3} G(k_1, k_2, k_3)$ and we extract the most negative eigenvalue of the matrix to represent the magnitude of this channel, $V_{pdw} = \min(eigenvals(-V))$. Similarly, all the k_1, k_2, k_3, k_4 which satisfy $k_1 - k_3 - q_{sdw} \mod 2\pi = 0$ and $k_4 - k_2 - q_{sdw} \mod 2\pi = 0$ will contribute to the spin-density-wave channel with $q_{sdw} = \pi$. $V_{sdw} = \min(eigenvals(V))$, where $V(k_1, k_4) = \sum_{k_2,k_3} G(k_1, k_2, k_3)$.

For charge-density-wave, it becomes a little bit complicated. All the k_1, k_2, k_3, k_4 which satisfy $k_1 - k_4 - q_{cdw} \mod 2\pi = 0$ and $k_3 - k_2 - q_{cdw} \mod 2\pi = 0$ contribute to V_1 where $V_1(k_1, k_3) = \sum_{k_2,k_4} -2G(k_1, k_2, k_3)$ and all the k_1, k_2, k_3, k_4 which satisfy $k_1 - k_3 - q_{cdw} \mod 2\pi = 0$ and $k_4 - k_2 - q_{cdw} \mod 2\pi = 0$ contribute to V_2 where $V_2(k_1, k_4) = \sum_{k_2,k_3} G(k_1, k_2, k_3)$. Therefore, $V_{cdw} = \min(eigenvals(V_1 + V_2))$.

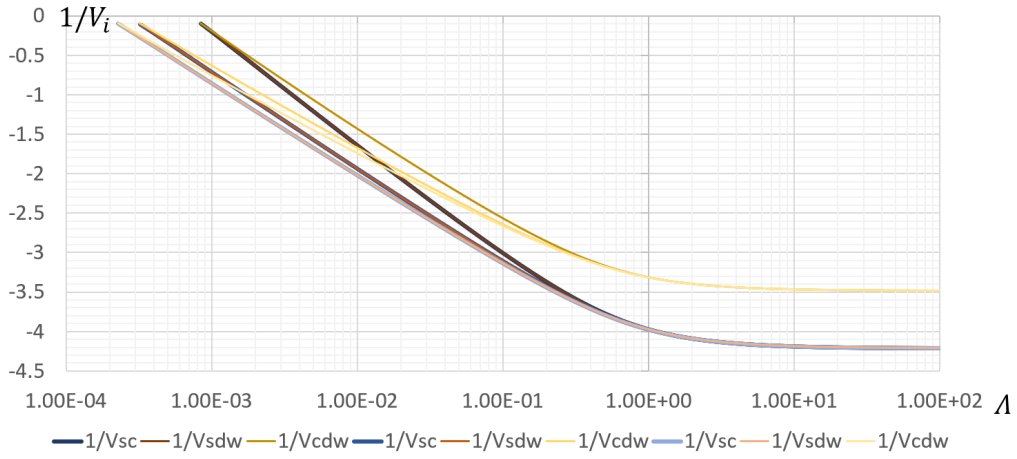

图 4-1: The patch FRG flow for $1/V_{sc}, 1/V_{sdw}, 1/V_{cdw}$ with 4 patches and $U = 0.125, V = -0.125, J = 0.7$. The 3 groups of the flow V_{sc}, V_{sdw} are for $k_{FL1} = 0.7\pi, 0.6\pi, 0.5001\pi$. At low energy scale, all the channels diverge and V_{sc}, V_{sdw} are degenerate with this initial condition. For different band structures, we see the flow diverges quickly when two fermi points are largely separated.

Fig. 4-1 shows the 4-patch FRG results. The Brillouin zone is divided into 4 patches correspond to the 4 fermi points. The inverses of the interactions in different channels versus log Λ have the "ray" like feature in a large range of the energy scale. For the band structure with largely separated fermi points, the flows will quickly diverge. When the two bands almost overlap, or to say, degenerate and flows diverge slowly, the system is more like a 1d chain.

For the different initial conditions, two of V_{sc}, V_{sdw}, V_{cdw} are degenerate and diverge at the same energy scale. Fig. 4-2 shows that the V_{sc}, V_{sdw} are degenerate with the initial condition on-site interaction $U = 0.125$, nearest-neighbor Coulomb interaction $V = -0.125$ and nearest-neighbor spin exchange $J = 0.7$. V_{sc}, V_{cdw} are degenerate with $U = 0.3, V = -0.1, J = 0.4$.

The previous results are for the 4 patch FRG, the "ray" like feature occurs in a

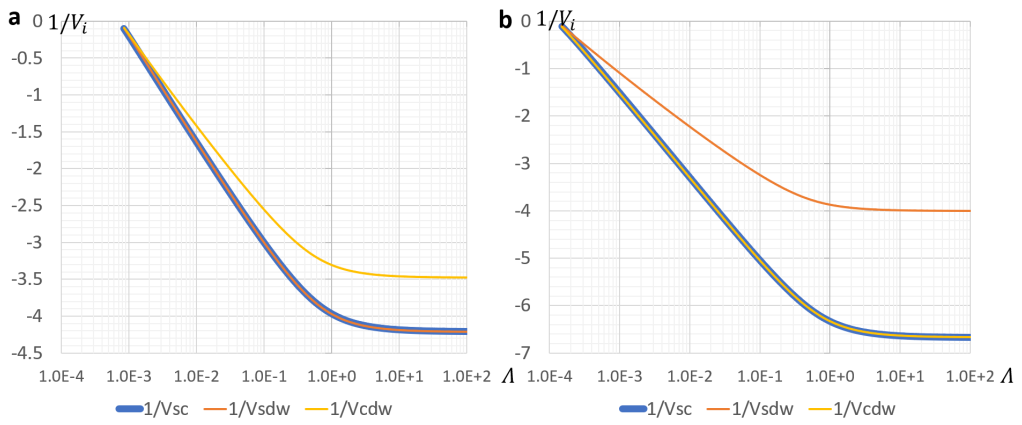

图 4-2: The patch FRG flow for $1/V_{sc}, 1/V_{sdw}, 1/V_{cdw}$ with 4 patches. **a** shows V_{sc}, V_{sdw} are degenerate with $U = 0.125, V = -0.125, J = 0.7$ while **b** shows V_{sc}, V_{cdw} are degenerate with $U = 0.3, V = -0.1, J = 0.4$. The flow for V_{sc} is a wider blue line for clarity.

large range of the energy scale. However, this is not true in the finer division of the momentum space, for example, adding more points around the fermi points. 4 patch FRG is an extremely coarse division of the momentum space and can be compared with the analytical results.

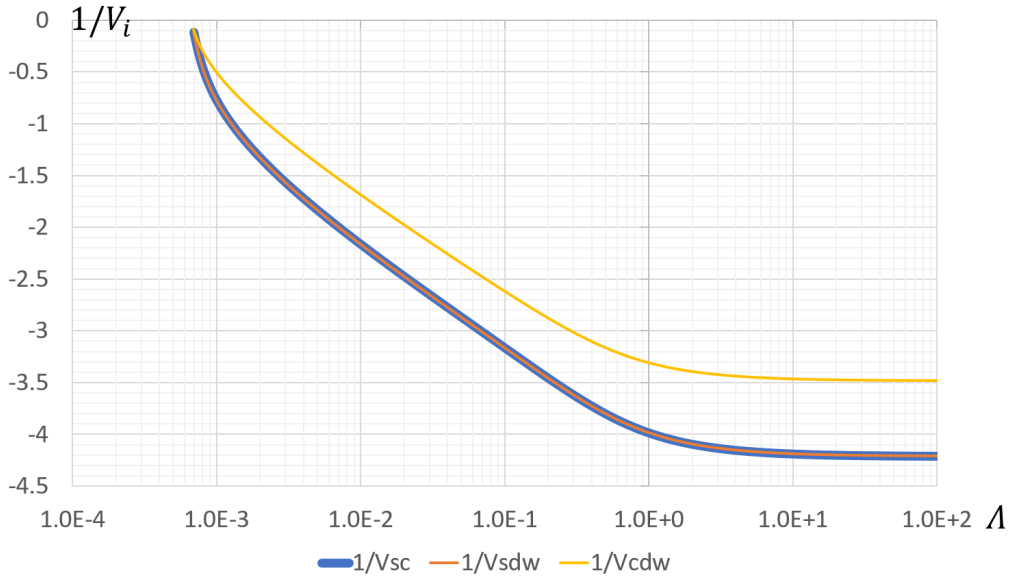

图 4-3: The patch FRG flow for $1/V_{sc}, 1/V_{sdw}, 1/V_{cdw}$ with 36 patches and $U = 0.125, V = -0.125, J = 0.7$. For each fermi points, there are additional 4 points on each side.

Apart from the analytical results, near the divergence, the "ray" like feature doesn't

occur in the 36 patches result. Fig. 4–3 and Fig. 4–4 clearly show the deviation from the "ray" like feature. Although the degeneration of V_{sc}, V_{sdw} still exist, the ratio of the interactions are no longer a constant.

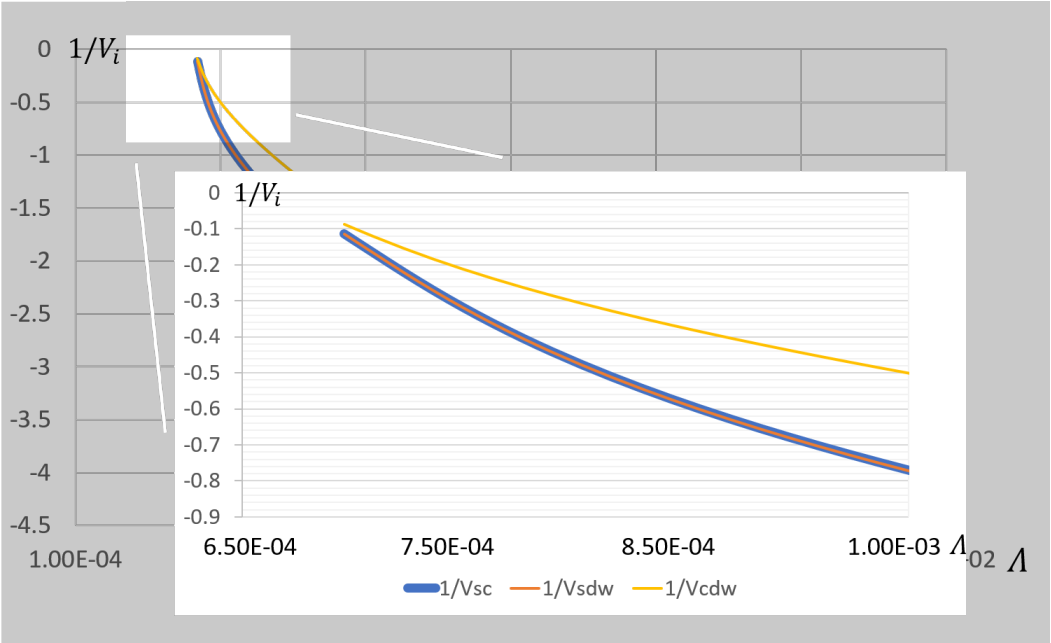

图 4–4: Zoom into the low energy window of the functional renormalization group flow for $1/V_{sc}, 1/V_{sdw}, 1/V_{cdw}$ with 36 patches and $U = 0.125, V = -0.125, J = 0.7$.

Fig. 4–5 shows the FRG flow with more patches, the deviation from the SO(8) symmetry becomes large. To characterise the deviation, we fit the curve by $a+bx+c/x$ and compute the deviation value $\eta = b/c$. Large $|\eta|$ represents more linear the curve is.

To compared with the SMFRG result, we set on-site interaction $U = 1$ and other interactions zero. The SO(8) symmetry is destroyed in this situation. Fig. 4–7 and Fig. 4–8 show the FRG flow with 4 and 60 patches. The spin-density-wave diverges fast in all the cases. However, with increasing the patches, the charge-density-wave and superconductivity diverges slowly. We can expect that the charge-density-wave and superconductivity remain small with the consideration of infinite number of patches.

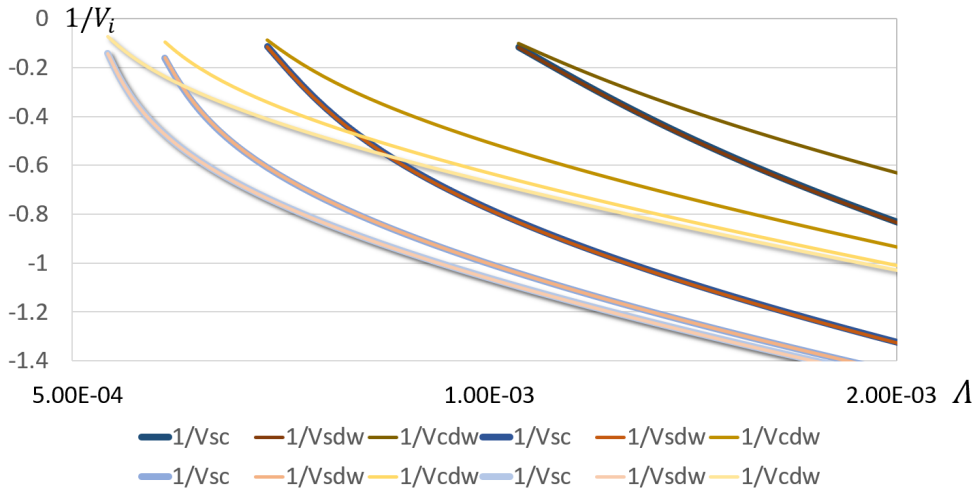

图 4-5: The patch FRG flow for $1/V_{sc}, 1/V_{sdw}, 1/V_{cdw}$ with 12, 36, 100, 196 patches and $U = 0.125, V = -0.125, J = 0.7$. Dark colors represent less patches, light colors represent more patches.

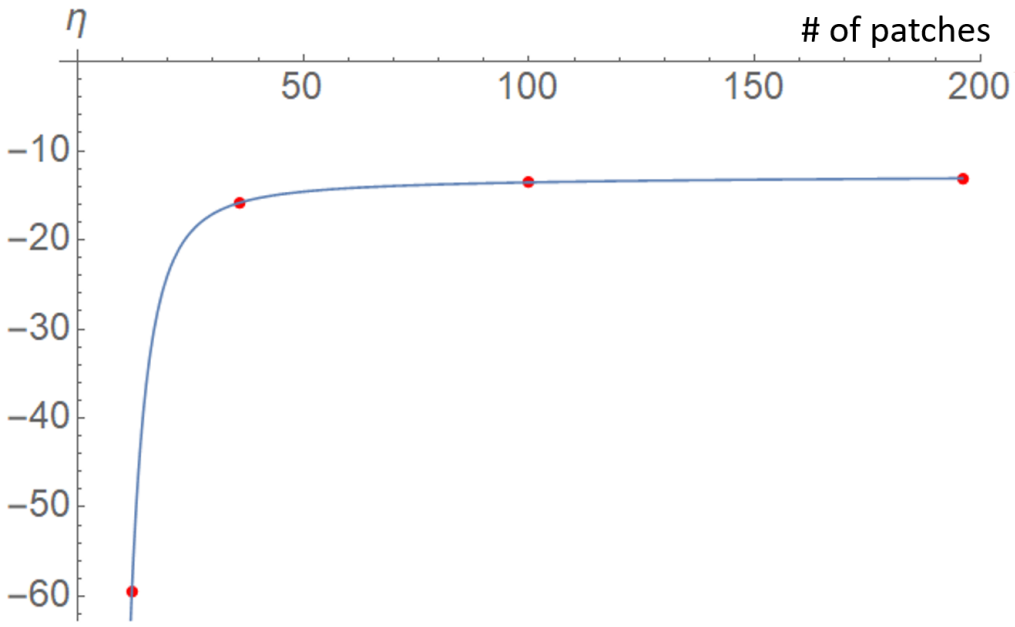

图 4-6: The deviation value η versus number of patches.

Arrange the vertex functions into current representation

Together with the definition in Eq. 2-7 and Eq. 2-8, the current representation of the interaction Eq. 2-9 can be represented by fermion creation and annihilation oper-

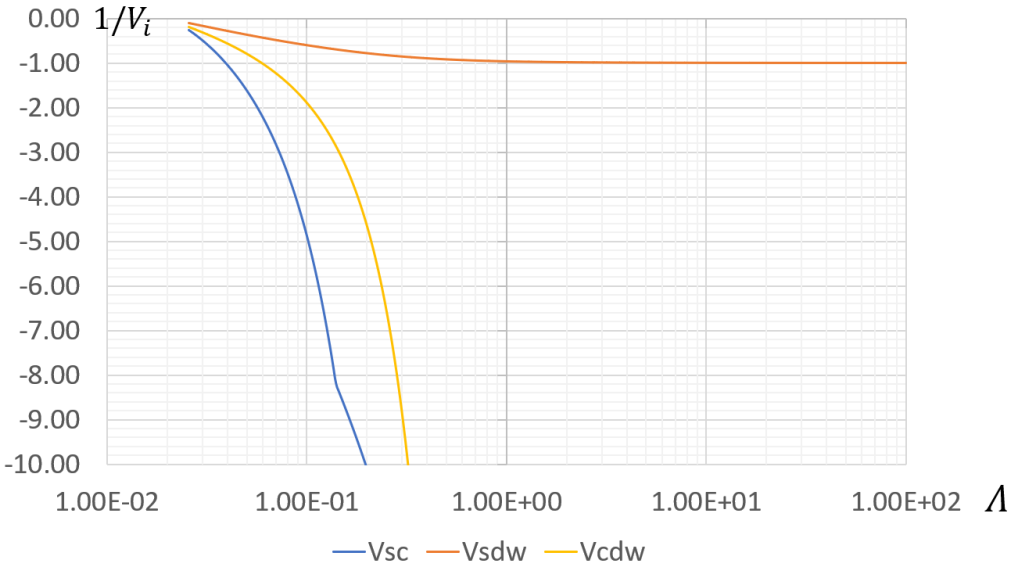

图 4–7: FRG flow for two-leg ladder with 4 patches and only on-site interaction $U = 1$.

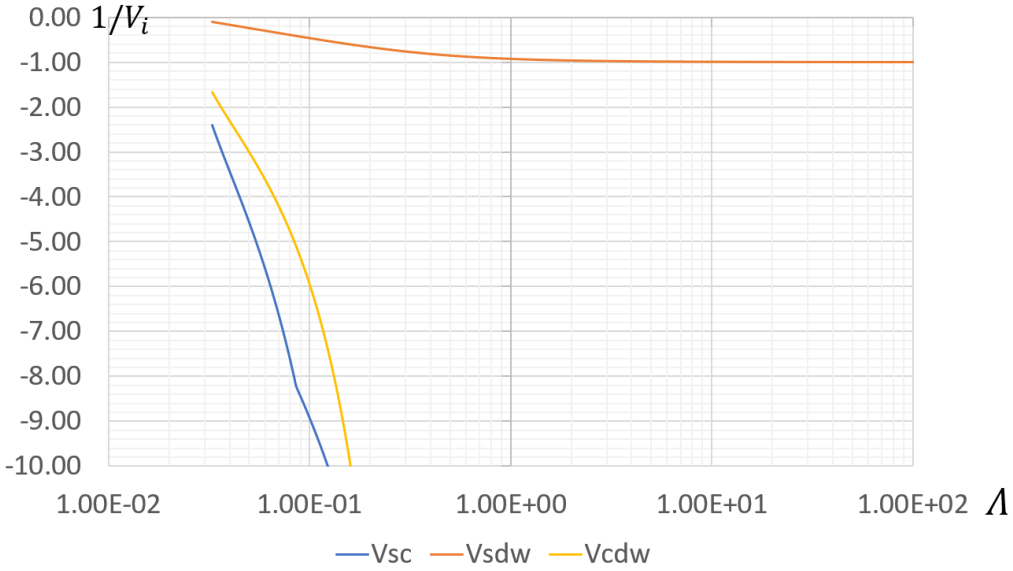

图 4–8: FRG flow for two-leg ladder with 60 patches and only on-site interaction $U = 1$.

ators,

$$
\begin{aligned}
\mathcal{H}_I &= b^{\rho}_{ij} c^{\dagger}_{Ri\alpha} c_{Rj\alpha} c^{\dagger}_{Li\beta} c_{Lj\beta} - \tfrac{1}{4} b^{\sigma}_{ij} \sigma^{k}_{\alpha\beta} \sigma^{k}_{\gamma\delta} c^{\dagger}_{Ri\alpha} c_{Rj\beta} c^{\dagger}_{Li\gamma} c_{Lj\delta} \\
&+ f^{\rho}_{ij} c^{\dagger}_{Ri\alpha} c_{Ri\alpha} c^{\dagger}_{Lj\beta} c_{Lj\beta} - \tfrac{1}{4} f^{\sigma}_{ij} \sigma^{k}_{\alpha\beta} \sigma^{k}_{\gamma\delta} c^{\dagger}_{Ri\alpha} c_{Ri\beta} c^{\dagger}_{Lj\gamma} c_{Lj\delta} \\
&+ u^{\rho}_{ij} \left(\varepsilon_{\beta\alpha} \varepsilon_{\gamma\delta} c^{\dagger}_{Rj\beta} c^{\dagger}_{Ri\alpha} c_{Li\gamma} c_{Lj\delta} + \varepsilon_{\alpha\beta} \varepsilon_{\delta\gamma} c^{\dagger}_{Lj\delta} c^{\dagger}_{Li\gamma} c_{Ri\alpha} c_{Rj\beta} \right) \\
&- \tfrac{1}{4} u^{\sigma}_{ij} \left(\varepsilon_{\beta\alpha} \sigma^{k*}_{\beta\alpha} \varepsilon_{\gamma\delta} \sigma^{k}_{\gamma\delta} c^{\dagger}_{Rj\beta} c^{\dagger}_{Ri\alpha} c_{Li\gamma} c_{Lj\delta} + \varepsilon_{\alpha\beta} \sigma^{k}_{\alpha\beta} \varepsilon_{\delta\gamma} \sigma^{k*}_{\delta\gamma} c^{\dagger}_{Lj\delta} c^{\dagger}_{Li\gamma} c_{Ri\alpha} c_{Rj\beta} \right),
\end{aligned}
\tag{4–1}
$$

where taking the Hermitian conjugate of the Pauli matrices yields, $(\sigma^k_{\alpha\beta})^\dagger = \sigma^{k*}_{\beta\alpha}$. Meanwhile, the vertex function with spin can be reconstructed from the coupling functions V_{k_1,k_2,k_3} by Eq. 3-4. The general interaction with fermion creation and annihilation operators can be expressed with the spinful vertex function,

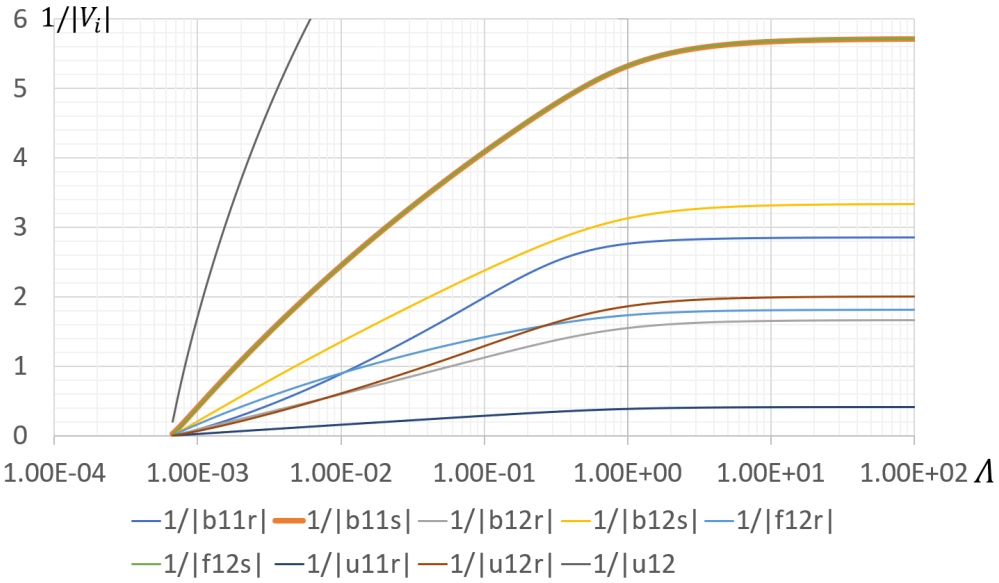

图 4-9: Functional renormalization group flow for $1/b^\rho_{11}, 1/b^\sigma_{11}$, $1/b^\rho_{12}, 1/b^\sigma_{12}$, $1/f^\rho_{12}, 1/f^\sigma_{12}$, $1/u^\rho_{11}, 1/u^\rho_{12}, 1/u^\sigma_{12}$ with 44 patches and $U = 0.125, V = -0.125, J = 0.7$.

$$\Gamma^\Lambda_{s_1,s_2,s_3,s_4}(K_1,K_2;K_3,K_4)c^\dagger_{K_4,s_4}c^\dagger_{K_3,s_3}c_{K_2,s_2}c_{K_1,s_1}.$$

Compared with the coefficients in Eq. 4-1, the forward, backward and umklapp scattering couplings can be expressed by the vertex function. Fig. 4-9 shows the flows for the nine independent couplings from the result of 44 patches FRG.

Results from SMFRG

The flows in SMFRG are for the particle-particle channel, particle-hole crossing and direct channels. It is natural to combine the channels and give the V_{sc}, V_{sdw}, V_{cdw}. Specifically, $V_{sc} = P, V_{sdw} = -C, V_{cdw} = -C + 2D$ and we use the most negative eigenvalues of V_{sc}, V_{sdw}, V_{cdw} to investigate the instability of each order.

Initially, we set the on-site interaction to be U, in this case, $P_{mn}(R = 0) = U, C_{mn}(R = 0) = U, D_{mn}(R = 0) = U$, and then Fourier transform them to the momentum space. Typically, the most negative eigenvalues in the 3 channels are, $V_{sc} = 0, V_{sdw} = -U, V_{cdw} = 0$. When lowering the energy scale, V_{sc}, V_{sdw}, V_{cdw} will diverge in half-filled two-leg ladder model and 1d chain model, or will change to a constant value (marginal) in 1d chain model deviated from half-filling.

SMFRG on two-leg ladder system

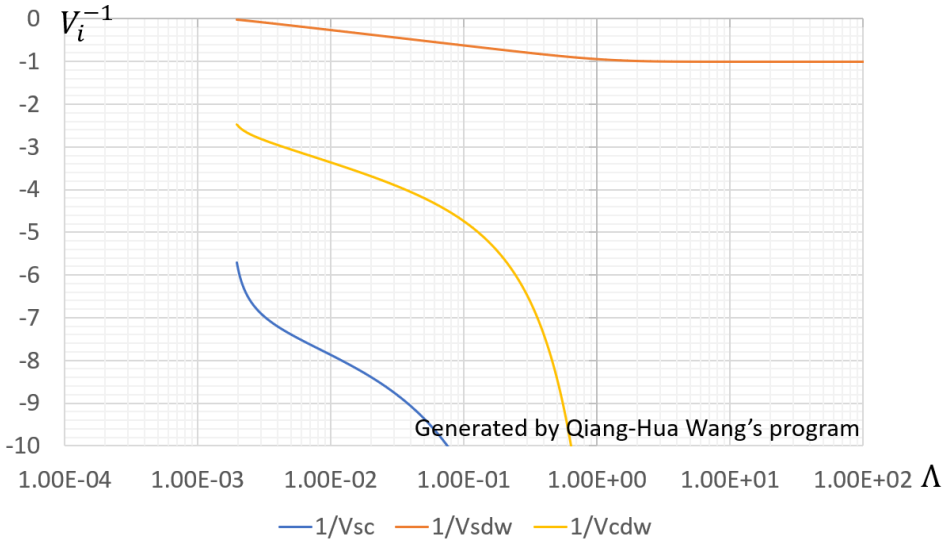

图 4–10: SMFRG flow for the two-leg ladder with half filling and $U = 1$, using on-site and nearest neighbour form factors.

In the calculation, the initial values are set, $U = 1, V = 0, J = 0$. Fig. 4–10 shows the SMFRG result for two-leg ladder chain. Here, we consider the on-site and nearest neighbour form factors. The spin-density-wave finally diverges and probably form the spin-density-wave order while superconductivity and charge-density-wave only have the tendency to diverge. At the final stage, we also investigate the eigenvectors and eigenvalues of each channel, which indicate the structure and transfer momentum of each channel. For the spin-density-wave, the transfer momentum $q = \pm\pi$. The Fourier transformation of the eigenvector is the real-space form factor and indicate the on-site spin-density-wave.

The results in SMFRG with only on-site and nearest neighbour form factor can be compared with the results in patch FRG with hundreds of patches. SMFRG compensate the disadvantage in patch FRG, such as considering more complete momentum dependence, because the momenta are projected onto the fermi surface and lose the radial dependence. Meanwhile, the reduced three channels correspond to the potential singular modes which finally lead to instability.

One can expect more diverse forms of charge-density-wave, spin-density-wave and superconductivity in two-leg ladder system than those in 1d chain, this is confirmed in SMFRG.

SMFRG on 1d chain

We also calculate the 1d chain model with half filling, in which $\mu = 0$. All the interactions diverge in this case and similar to the case in two-leg ladder. The divergences of spin-density-wave, superconductivity and charge-density-wave onset at different energy scales. $1/V_{sdw}$ has the "ray" like feature and finally diverges at 10^{-4}. The most negative eigenvalues comes from $q = \pm\pi$, indicating the transfer momentum $q_{sdw} = \pm\pi$. The eigenvectors of the matrices V_{sc}, V_{sdw}, V_{cdw} indicate the form of these orders. At the stage when diverging, we Fourier transform the eigenvectors and yield that the spin-density-wave occurs on-site.

To understand the SMFRG, we first consider only on-site form factor, therefore, the number of sublattice and form factor all equal to 1. The Green function is,

$$G(\omega, k) = \frac{1}{i\omega - (-2\cos k + \mu)}.$$

We first ignore the channel overlaps, which means we do not project other channels to the flow equation. This is the random phase approximation. Fig. 4–11 shows all the interactions are marginal, which agrees with the analytical results. When considering the channel overlaps, the result also shows the all the interactions are marginal, but the flows in the intermediate region are different.

Next we consider the channel overlaps, the other channels will be projected to the

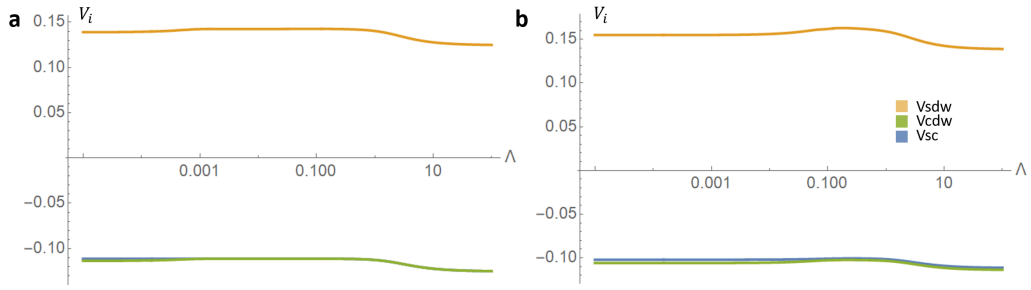

图 4-11: SMFRG flow for the 1d chain without channel overlaps. This is the random phase approximation. **a** shows the results from numerical integrate the bubbles, **b** shows that from summing over the uniform discrete momentum points.

flow equation when the center of mass's distance R is small. Channels at $R = 0$ are strongly overlapped, which can be expressed as,

$$dP^{abcd}_{mn}(R=0) = \partial P^{abcd}_{mn}(R=0) + \partial C^{abcd}_{mn}(R=0) + \partial D^{abcd}_{mn}(R=0).$$

The full projection of the channel can be found by following Eq. 3-13, Eq. 3-14, Eq. 3-15, Eq. 3-16. Fig. 4-12 shows the SMFRG flow with the channel overlaps, all the interactions are marginal, but the superconductivity channel and charge-density-wave channel are separated.

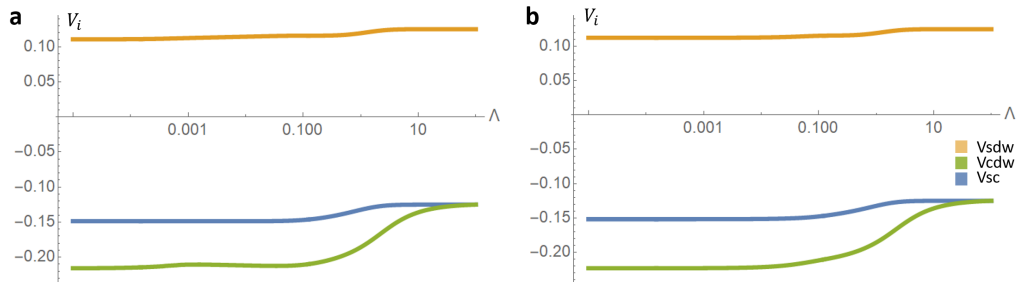

图 4-12: SMFRG flow for the 1d chain. **a** shows the result from numerical integrate the bubbles, **b** shows that from summing over the uniform discrete momentum points.

A further step in 1d chain, we include the nearest neighbours to the form factor, $f_m(k) = \{1, e^{-ik}, e^{ik}\}/(2\pi)$. The channel overlaps now extends to $R = \pm 2$. Fig. 4-13 shows the SMFRG flow for the 1d chain with the nearest neighbours, the deviation from the initial value becomes small. We can expect that with the consideration of next nearest neighbours and next-next nearest neighbours, the deviation becomes smaller.

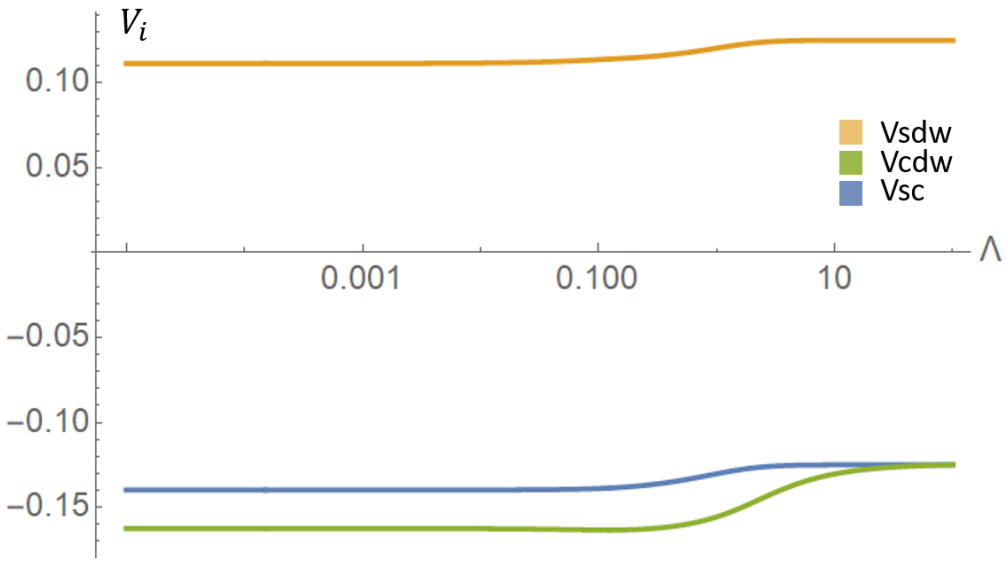

图 4-13: SMFRG flow for the 1d chain with nearest neighbours contribution.

Calculation errors

Recalling how we calculate the bubble in FRG, we only integrate a small region near the momentum points. However, in SMFRG, we integrate the the bubble in the entire Brillouin zone. This would cause large calculation errors. Fig. 4-14 shows the integrand with $\omega = 0.1, q = 0.4\pi$. The peaks need careful treatment especially in the sum scheme, otherwise, it will lead to large errors.

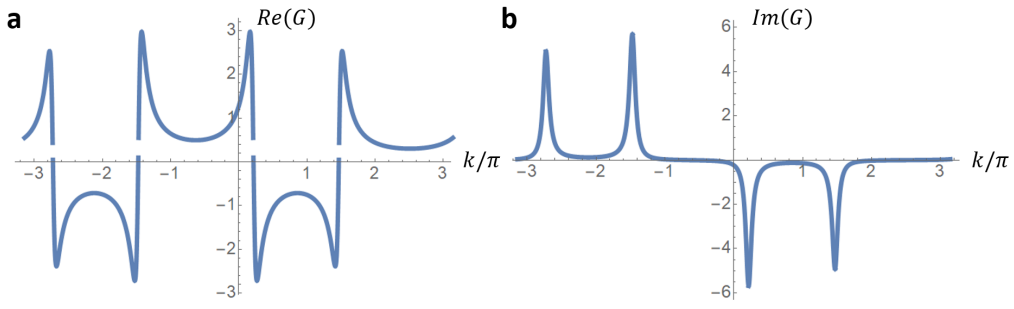

图 4-14: The integrand in the bubble calculation. **a** shows the real part of the integrand, **b** shows the imaginary part of the integrand.

Instead of uniformly distributing the momentum points, one can have more points

near the peaks. We dub the uniform distribution of the momentum points as $d_0(p) = p$. But for the sophisticated distribution $d(p)$, the Jacobian is needed to ensure the correctness of the integration, also the Fourier transformation and inverse fourier transformation.

If one import numerical integration package, the integration still doesn't give reasonable results if not treating the peaks carefully. Taking the 1d chain as an example, the integrands for the particle-particle bubble and particle-hole bubble are,

$$\chi_{pp/ph} = \frac{\pm\Lambda^2 + (\mu - 2\cos k)\,(\mu - 2\cos(k+q))}{\left(\Lambda^2 + (-2\cos k + \mu)^2\right)\left(\Lambda^2 + (-2\cos(k+q) + \mu)^2\right)}$$

where μ is the chemical potential and Λ is the frequency cutoff. The Λ ensures the convergence of the integration of momentum k, but one still have to treat k near $-2\cos k + \mu$ and $-2\cos(k+q) + \mu$ carefully.

In practice, we divide the domain into subranges, small subranges enclose the peaks. We integrate the integrand in the subranges and then sum up.

Conclusion

In this thesis, we use functional renormalization group (FRG) and singular mode renormalization group (SMFRG) to investigate the two-leg ladder model. We find that with the finer grid of the momentum space, the results deviate from the exact SO(8) symmetry of the interactions. Near the divergence, the ratio of each interaction is not a constant anymore and the "ray" feature disappears. SMFRG yields the results correspond to the patch FRG with large number of patches. Meanwhile, the form factors yield the final stage may develop on-site spin-density-wave order. We also use the SMFRG method to review the 1d chain model with half-filling and deviates from half-filling. We find that all the interactions are marginal when the system deviates from half filling and the interactions diverge like those in two-leg ladder when the system is half-filling.

Summary of implementation of FRG and SMFRG

We developed the FRG and SMFRG in a detailed way.

For FRG, the implementation is relatively simple. At each step, we integrate the bubble over a small region near the momentum points and use the five Feynman diagram to calculate the flow of SU(2) invariant vertex functions. The flow of the vertex functions can be rearranged into superconductivity channel, spin-density-wave channel, and charge-density-wave channel. Also, the vertex function can be arranged into currents to represent forward scattering, backward scattering, and umklapp scattering. We also find that different initial values lead to two degenerate flows in the 3 channels.

For SMFRG, we decompose the vertex function into three channels. The five Feynman diagrams in FRG contribute to the three channels respectively. Particle-particle for the P channel, particle-hole crossing for the C channel and particle-hole direct for the D channel. With the form factor, the bubbles are calculated by summation

or numerical integration over the entire Brillouin zone. An extra step is to investigate the channel overlaps. In real space, with small R, different channels contribute to the same vertex function. One has to Fourier transform the channel into real space and then project other channels to the flow equation. With inverse Fourier transformation, the correct flow equations are obtained. Initially, in real space, each channel has on-site interaction U, we do inverse Fourier transformation to find the channels in momentum space. At the final stage, we investigate the eigenvectors of the diverged channel, and Fourier transform them to investigate the real space pattern.

Summary of two-leg ladder Hubbard model

Two-leg ladder Hubbard model is a quasi-1d strongly correlated system. The special geometry lattice not only can be solved by both analytical and numerical method but also yields many new physics. Because of the tendency to form singlet on the rungs, it has a special Mott phase with a spin gap. The renormalization group methods derive the flow equation for 9 independent interactions. At low energy scale, two of them remain small and the other 7 interactions flow with the constant ratio and have "ray" like feature. The low energy effective theory can be exactly mapped to the SO(8) Gross-Neveu (GN) model. The SO(8) generators mix the superconductivity, spin-density-wave and charge-density-wave.

Our N-patch functional renormalization group method shows that the features fade away when considering finer momentum grid, which means divide the momentum space into more patches. The linearity of $1/V_i$ rapidly decrease when increasing the patches. We also find the SO(8) symmetry strongly depends on the initial conditions. Besides grouping the vertex function into superconductivity, spin-density-wave and charge-density-wave, we also map them into the current representation and investigate the flow for the nine independent interactions.

参考文献

[1] HIRSCHFELD P, KORSHUNOV M, MAZIN I. Gap symmetry and structure of Fe-based superconductors[J]. Reports on Progress in Physics, 2011, 74(12): 124508.

[2] STEWART G. Non-Fermi-liquid behavior in d-and f-electron metals[J]. Reviews of Modern Physics, 2001, 73(4): 797.

[3] BEDNORZ J G, MÜLLER K A. Possible highT c superconductivity in the Ba-La- Cu- O system[J]. Zeitschrift für Physik B Condensed Matter, 1986, 64(2): 189 – 193.

[4] SCHILLING A, CANTONI M, GUO J, et al. Superconductivity above 130 K in the Hg–Ba–Ca–Cu–O system[J]. Nature, 1993, 363(6424): 56.

[5] LEE P A, NAGAOSA N, WEN X-G. Doping a Mott insulator: Physics of high-temperature superconductivity[J]. Reviews of modern physics, 2006, 78(1): 17.

[6] ZHANG F, RICE T. Effective Hamiltonian for the superconducting Cu oxides[J]. Physical Review B, 1988, 37(7): 3759.

[7] LAKE B, AEPPLI G, MASON T, et al. Spin gap and magnetic coherence in a clean high-temperature superconductor[J]. Nature, 1999, 400(6739): 43.

[8] RICE T, GOPALAN S, SIGRIST M. Superconductivity, spin gaps and Luttinger liquids in a class of cuprates[J]. EPL (Europhysics Letters), 1993, 23(6): 445.

[9] LIN H-H, BALENTS L, FISHER M P. Exact SO (8) symmetry in the weakly-interacting two-leg ladder[J]. Physical Review B, 1998, 58(4): 1794.

[10] TROYER M, WIESE U-J. Computational complexity and fundamental limitations to fermionic quantum Monte Carlo simulations[J]. Physical review letters, 2005, 94(17): 170201.

[11] LIU Y-H, WANG W-S, WANG Q-H, et al. Transformation of the superconducting gap to an insulating pseudogap at a critical hole density in the cuprates[J]. Physical Review B, 2017, 96(1): 014522.

[12] ZANCHI D, SCHULZ H. Weakly correlated electrons on a square lattice: Renormalization-group theory[J]. Physical Review B, 2000, 61(20): 13609.

[13] HALBOTH C J, METZNER W. Renormalization-group analysis of the two-dimensional Hubbard model[J]. Physical Review B, 2000, 61(11): 7364.

[14] DAGOTTO E, RICE T. Surprises on the way from one-to two-dimensional quantum magnets: the ladder materials[J]. Science, 1996, 271(5249): 618 – 623.

[15] DAGOTTO E, RIERA J, SCALAPINO D. Superconductivity in ladders and coupled planes[J]. Physical Review B, 1992, 45(10): 5744.

[16] MARKIEWICZ R, VAUGHN M T. Stripes, pseudogaps, and SO (6) in the cuprate superconductors[J]. Journal of Physics and Chemistry of Solids, 1998, 59(10-12): 1737 – 1741.

[17] SHANKAR R. Renormalization-group approach to interacting fermions[J]. Reviews of Modern Physics, 1994, 66(1): 129.

[18] METZNER W, SALMHOFER M, HONERKAMP C, et al. Functional renormalization group approach to correlated fermion systems[J]. Reviews of Modern Physics, 2012, 84(1): 299.

[19] HUSEMANN C, SALMHOFER M. Efficient parametrization of the vertex function, Ω scheme, and the t, t' Hubbard model at van Hove filling[J]. Physical Review B, 2009, 79(19): 195125.

[20] WANG W-S, XIANG Y-Y, WANG Q-H, et al. Functional renormalization group and variational Monte Carlo studies of the electronic instabilities in graphene near 1 4 doping[J]. Physical Review B, 2012, 85(3): 035414.

[21] LIN H-H, BALENTS L, FISHER M P. N-chain Hubbard model in weak coupling[J]. Physical Review B, 1997, 56(11): 6569.

[22] BALENTS L, FISHER M P. Weak-coupling phase diagram of the two-chain hubbard model[J]. Physical Review B, 1996, 53(18): 12133.

[23] WILSON K G. The renormalization group: Critical phenomena and the Kondo problem[J]. Reviews of modern physics, 1975, 47(4): 773.

[24] POLCHINSKI J. Renormalization and effective Lagrangians[J]. Nuclear Physics B, 1984, 231(2): 269–295.

科研成果

1. Li, J., Pereira, P. J., Yuan, J., Lv, Y. Y., Jiang, M. P., Lu, D., ... & Ke, X. (2017). Nematic superconducting state in iron pnictide superconductors. *Nature communications*, 8(1), 1880.
2. Lu, D. C., Lv, Y. Y., Li, J., Zhu, B. Y., Wang, Q. H., Wang, H. B., & Wu, P. H. (2018). Elliptical vortex and oblique vortex lattice in the FeSe superconductor based on the nematicity and mixed superconducting orders. *npj Quantum Materials*, *3*(1), 12.
3. Sun, H., Lv, Y., Lu, D., Yang, Z., Zhou, X., Hao, L., ... & Xu, W. (2017). Intrinsic superconducting transport properties of ultra-thin $Fe_{1+y}Te_{0.6}Se_{0.4}$ microbridges. *SCIENCE CHINA Physics, Mechanics & Astronomy*, *60*(11), 117411.
4. Bao, W. C., Tang, Q. K., Lu, D. C., & Wang, Q. H. (2018). Visualizing the $ d $-vector in a nematic triplet superconductor. *arXiv preprint arXiv:1804.10148*.

致　谢

转眼间，我已经快要毕业了。回首过去的四年，我非常感谢所有帮助过我，支持过我的人。

大四这一年，我主要学习了泛函重整化群及其推广，并完成了我的本科毕业论文。在这里，我首先非常感谢我的导师，王强华教授，他不光教会我许多知识，更使我明晰了未来的研究方向。与他的讨论往往使我受益匪浅，给我许多研究上的启发，并帮助我度过难关。王老师严谨的治学精神也是我要不断学习努力达到的。\par

感谢南京大学提供的平台，让我在本科四年中能接触物理学的许多方向，从高能到凝聚态，从实验到理论。感谢我的挚友孙正迪同学在大一上跟我讲规范场理论、广义相对论，让我知道了弦振动方程以外的物理世界。在本科期间，我们时常讨论理论物理问题，很幸运能遇到这样一位志同道合的同学。

感谢电子学院的李军老师一直以来对我支持与帮助，为我提供出国交流的机会，以及耐心的修改我的文章，使得我的论文得以顺利发表。

感谢闻海虎教授，张若昀教授，吴盛俊教授，James Analytis教授对我学业上的帮助，这些精彩的课程使我受益匪浅。也为我今后的科研打下了良好的基础。感谢王思慧教授组织物理学术竞赛，让我在大一初尝科研的感觉。

此外，还要感谢我的室友欧先飞、曹云浩同学对我Ubuntu使用和LaTeX编译上的帮助，感谢我的父母对我生活上的支持与关照。感谢宋瑞珩同学在课余陪我打球，让我在大四依然能有比较好的身体素质。

回首本科四年，除了学业，科研，交流，运动之外，我的心境也发生了改变，希望在未来的道路上，我能继续砥砺奋进，攀登理论物理科研的高峰。